Analytical Micro-Modeling of Masonry Periodic Unit Cells – Elastic Properties

Anastasios Drougkas[1], Pere Roca, Climent Molins

Departament d'Enginyeria de la Construcció, Universitat Politècnica de Catalunya, Campus Diagonal Nord, Building C1, Jordi Girona 1-3 UPC, 08034 Barcelona, Spain

Highlights

- The mechanical properties of masonry composites are derived from PUC calculations
- Several different masonry wall and pillar typologies are investigated
- The orthotropic elastic characteristics are determined with very low computational cost
- The numerical results are compared to experimental data
- A parametric investigation is performed to determine the accuracy of the model compared to FE calculations

Keywords

Micro-modeling; analytical modeling; masonry; elastic moduli

1. Introduction

1.1 State of the Art

Masonry structures currently constitute a very large part of the existing built environment. They include a large amount of common but still-in-use buildings as well as outstanding cultural heritage structures. Masonry buildings are comprised of structural members such as load bearing walls, pillars and vaults composed of single

[1] Corresponding Author
Email addresses: anastasios.drougkas@upc.edu (Anastasios Drougkas), pere.roca.fabregat@upc.edu (Pere Roca), climent.molins@upc.edu (Climent Molins)

or multiple brick or stone masonry leaves with possible interior rubble infills. An accurate structural analysis of such buildings is important as a way to verify their capacity against gravity loads and horizontal actions such as wind and earthquake. However, the structural analysis of masonry buildings faces significant challenges due to the complex behavior of masonry which stems from its composite character, the influence of the geometric arrangement of units and the fact that most utilized mortars only provide a weak bond between units. One of the consequences of the composite nature of masonry is found in its anisotropic mechanical response. Another emerging consequence is the difficulty of predicting the average masonry mechanical properties, such as, in particular, the masonry compressive strength and the Young's modulus, from the properties of the constituent materials. Even when the elastic properties of the constituent materials are known, it is difficult to derive the elastic properties of the composite without resorting to sophisticated analysis tools. Furthermore, results for one masonry typology may not be readily suitable for the evaluation of the properties of another. Therefore, the development of simple tools for the derivation of the orthotropic elastic properties of a variety of masonry typologies based on the elastic properties of their constituent materials, while maintaining a single analysis methodology throughout, constitutes a sound framework for the further development of analysis tools based on the detailed micro-modeling approach.

Masonry structures composed of periodically repeating patterns may be simplified in order to facilitate their analysis. In this sense, it is possible to calculate the elastic and strength properties of masonry structures through the analysis of a geometrically repeating part. This part may be further simplified by taking into account symmetry arising from geometrical and loading conditions.

A number of analytical and numerical models has been proposed for the analysis of masonry periodic unit cells using a variety of methods. These have been employed for the derivation of the elastic and inelastic properties of masonry composites as a result of the interaction of their two phases: units and mortar. The cells are analyzed considering appropriate boundary conditions, kinematic compatibilities and stress equilibrium in order to derive the strains and stress state in the cell for different loading conditions. Nonlinear properties may be derived from the iterative solution of the problem under the assumptions of plasticity or damage models for the behavior of the materials in the cell.

Through these computations in the micro- or meso-scale it is possible to calculate the orthotropic behavior of the masonry composite in the macro-scale, arising from the geometrical arrangement of the two phases in the cell. Elastic [1–4] and strength properties [5–8] of the composite for in-plane and out-of-plane load conditions have been calculated using such techniques. Research has extended from the study of periodic masonries to non-periodic masonries [7,9].

Methods for the analysis of masonry cells using analytical methods have been proposed, mostly focusing on the analysis of stack bond and running bond masonry wall typologies [4,10,11]. Finite element representations of masonry unit cells have also been proposed [12] in which the interaction of the two phases, the resulting stress and strains in the cell and the nonlinear behavior of the materials may be accurately represented. This approach has also been adopted for the verification of the accuracy of analytical models, such as the ones already described, the production of in-plane strength domain curves for masonry membranes and the execution of two-scale analyses. However, FE calculations may require time for the creation of the models and high computational effort. A comparison of analytical model and FE model results may be found in [3].

A micromechanical approach for the analysis of periodically reinforced composites, according to which a repeating cell of the composite is discretized into sub-cells with different properties and arranged in a regular grid, has been proposed in the past [13]. Equilibrium and compatibility conditions are assembled in a set of closed form expressions and can be solved in a single analysis step for the derivation of, for example, the average elastic properties of the composite. The benefit of this approach is its computational efficiency and relative simplicity. Masonry periodic unit cells, seen as regular arrangements of square or cubic sub-cells with different material properties, can be analyzed using the same approach. Adaptations of this method, capable of providing closed form expressions for the elastic properties of stack and running bond masonry, have been proposed [14,15].

Masonry analyzed in this manner is usually idealized as an infinitely thin or infinitely thick membrane, these assumptions being accordingly equivalent to a plane stress and plane strain approach. However, the existence of transversal joints, gaps or other discontinuities, which result in non-constant geometric structure along the depth of the masonry, render these two approaches fundamentally not accurate. Analysis of the unit

cell taking into account these discontinuities must consider the actual finite thickness and actual geometry of the masonry structure.

Computations on cells where the actual finite thickness of the masonry is considered allow for a more accurate representation of out-of-plane stresses, which, while only marginally affecting the initial elastic stiffness, may strongly influence the compressive strength of the composite [16]. However, since it is intended to apply the models proposed here in nonlinear analysis in a following paper, it is deemed necessary to include a realistic representation of the out-off-plane stresses using three-dimensional models for linear elastic analysis as well. With this type of models, the true thickness of the masonry may be easily taken into account in finite element calculations.

Through computations on periodic unit cells it is possible to make fairly accurate predictions of the compressive and tensile strength and the elastic moduli of masonry. Such techniques may be, therefore, used for two-scale modeling of masonry walls [17–21].

1.2 Objectives

The purpose of this paper is to present a simple analytical calculation method for the derivation of the elastic characteristics of masonry structures. The method is based on the analysis of masonry periodic unit cells, the smallest repeating geometrical entity representative of the overall masonry geometric pattern, in an attempt to derive masonry composite orthotropic macro-properties from material and geometrical micro-properties. The micro properties considered are those of the units, the mortar and the infill. Structural members allowing this type of modelling include single- and multi-leaf walls and pillar-like structures. These properties are to be determined for normal and shear loading. The models are formulated based on three-dimensional elasticity in order to include the influence of out-of-plane stresses on the response.

These macro-properties may be used for the analysis of large walls and other structures in full multi-scale models or may be used to provide the information needed for analysis with orthotropic material models, such as the Hill, Rankine-Hill or the Hoffmann criteria. The computational cost associated with FE analysis of cells in two-scale analyses is still relatively high, especially when the analyses are carried out on cells in a three-dimensional configuration. Analytical models for the analysis of the cells present an advantageous, in terms of

computational cost, alternative. Finally, the low computational cost of such analytical models makes the production of large databases of results undemanding.

The verification of the model is performed through a comparison against a FE result benchmark following a parametric investigation. A comparison is also carried out with a range of results from the existing inventory of experimental data.

This study includes the analysis of various masonry wall geometrical typologies: single leaf stack bond, single-leaf running bond, double-leaf Flemish bond and three-leaf walls with a running bond outer leaf. In the last case, the infill constitutes a third material phase, with different mechanical properties from the units and mortar normally considered in such analyses. These masonry typologies, and especially the last three, represent a significant portion of existing and new structures, with the available research focusing primarily, if not entirely, on running rather than Flemish bond structures. Three-leaf walls with rubble infill are also commonly encountered both in large structures and common buildings. Stack bond pillars are commonly used as specimens for experimental investigation, therefore a large body of experimental work exists dealing with their elasticity and strength properties. English bond prisms are similarly used for experimental investigation purposes as well as in structural practice. The study focuses on masonries characterized by units with an elastic stiffness higher than that of the mortar. However, the applicability of the model is examined through an analysis of experimental case studies with a wide range of properties. It has been noted that there is a lack of experimental results concerning the horizontal and transversal Young's moduli, the shear moduli and the Poisson's ratios of masonry in experimental cases which include also a detailed mechanical characterization of the units and mortar. This lack of experimental results has been compensated by using finite element results as benchmark cases.

2. Overview of the Models

2.1 Derivation of Wall Periodic Unit Cells

The derivation of the periodic unit cell is accomplished through the identification of the repeating pattern in the structure and its subsequent simplification due to symmetry conditions. The four masonry typologies studied, in order of complexity, are stack bond, running bond, Flemish bond and three-leaf masonry with a

running bond outer leaf and infill. The derivation patterns for the masonry wall typologies considered in this work are shown in Figure 1.

Stack bond and running bond walls are single leaf structures with no variation of the geometry along the thickness. Flemish bond walls include a thin transversal joint and the units are oriented as either header or stretcher blocks, meaning that for the largest portion of the wall the geometry changes along the thickness. Three-leaf walls are composed of outer leaves of any type and an interior leaf whose thickness may be larger than that of the outer leaves.

Increase in the geometrical complexity of the composite results in an increase in the size of the repeating pattern and, therefore, of the unit cell. In stack bond and running bond masonry the layout of the masonry does not change through the thickness and all units are identically oriented, while in Flemish bond masonry the mid-thickness is characterized by a transversal mortar joint and intersecting header units.

The anisotropic behavior of the masonry composite is the result of the geometrical arrangement of components, which are here considered isotropic, although the orthotropic behavior of bricks may be implemented with only minor alterations in the model. The infill is also considered macroscopically isotropic and is normally more deformable than the outer leaf.

2.2 Derivation of Pillar Periodic Unit cells

The periodic unit cells for pillar-like structures are derived similarly to the wall typologies. Two different structural types are considered: stack bond prisms and English bond pillars. The derivation of the cells is shown in Figure 2.

2.3 Discretization of the Derived Cells

The analytical model for the analysis of masonry periodic unit cells is based on the discretization of the cell in structural parts, the modeling of their interaction in terms of deformation and stress distribution and equilibrium under external loads. The equilibrium problem will be primarily solved for three normal stress components, σ_{xx}, σ_{yy} and σ_{zz} and six shear stress components, σ_{xy}, σ_{xz}, σ_{yx}, σ_{yz}, σ_{zx} and σ_{zy} in order to obtain the elastic properties of the cells in the three orthogonal directions dictated by the geometric arrangement of the masonry.

The discretization of the periodic unit cells is done as illustrated in Figure 3. It results in each cell being discretized into cuboid parts of units, bed joints, head joints, transversal joints, cross joints and infill. Specifically: the stack bond cell is discretized into one stretcher unit, one bed joint, one head joint and one cross joint part; the running bond cell is discretized into four stretcher unit, one bed, two head and two cross joint parts; the Flemish bond cell is discretized into four header unit, six stretcher unit, three bed joint, four head joint, seven cross joint and six transversal joint parts; the three-leaf cell is discretized similarly to the way the running bond cell with the addition of nine transversal joint parts representing the infill. The stack bond pillar is discretized into a unit part and a mortar part arranged in a layered pattern and the English bond pillar is discretized into four unit parts, one bed joint part two head joint parts and four cross joint parts.

The orthogonal discretization carried out separates the cell into parts allocated in an orthogonal grid, with each part belonging in one horizontal, one vertical and one transversal strip of cuboid parts. As a result, the stack bond cell is divided into two horizontal, two vertical and two transversal strips, the running bond cell into three horizontal, three vertical and six transversal strips and the Flemish bond cell into six horizontal, ten vertical and fifteen transversal strips. The type of the loading applied on the cell and its orientation compared to the orthogonal grid dictates the assumptions made for the elastic analysis of the cell, which are based on the strains to which each strip is subjected. The proposed discretization of mortar joints and units allows for simplified assumptions in the formulations of the model. The final discretization scheme is show in Figure 3.

3. Development of the Analytical Model

3.1 General Assumptions and Equations

The deformation of the cell faces, and, therefore, the total strain of the cell, depends on the loading applied. Application of normal stress results only in normal global cell strains and the application of shear stress results only in shear global cell strains. This means that under normal stress the total deformation of all strips, or the average strain of each one, is equal in the three principal directions.

Under the application of normal stress, either only normal or both normal and shear stresses may arise in the cuboid parts. In turn, under the application of shear stress, only shear stresses of the same geometrical orientation arise in the cuboid parts. All stresses and strains are assumed constant in the cuboid parts. For linear

elastic analysis, the units and the mortar are modeled as three-dimensional isotropic continua. Perfect bond is considered at the unit-mortar interface for the linear elastic computations performed here, so that all deformation of the cell is accounted for in the units, mortar and infill.

Isotropic linear elasticity stress-strain relations in three dimensions apply for every cuboid component under normal and shear stress. This includes the units, the mortar and the infill. These relations are expressed as:

$$\varepsilon_{ii,n} = \sigma_{ii,n} / E_n - \nu_n \left(\sigma_{jj,n} + \sigma_{kk,n} \right) / E_n \tag{1}$$

$$\varepsilon_{ij,n} = \sigma_{ij,n} \left(1 + \nu_n \right) / E_n \tag{2}$$

where the sub-index n refers to the identifier of the cuboid, σ_{ii} and ε_{ii} are the applied normal stress and calculated normal strain along axis i, σ_{ij} and ε_{ij} are the shear stress and strain in plane ij, E_n is the Young's modulus and ν_n is the Poisson's ratio.

When a cuboid with dimensions D_i and D_j is subjected to a shear stress σ_{ij} the contribution of the shear deformation of the cuboid d_i^{ij} to its normal deformation in the direction i is taken as being half the displacement at its top due to the shear stress. Therefore, it is defined as

$$d_i^{ij} = \varepsilon_{ij,n} \frac{D_j}{2} \tag{3}$$

The three Young's moduli for each cell configuration are calculated by use of the equation

$$E_{c,i} = \sigma_{ii} / \varepsilon_{ii} \tag{4}$$

The Poisson's ratios are determined by the equation

$$\nu_{c,ij} = -\varepsilon_{jj} / \varepsilon_{ii} \tag{5}$$

The three shear moduli for each cell configuration are calculated by use of the equation:

$$G_{c,ij} = \sigma_{ij} / \left(2\varepsilon_{ij} \right) \tag{6}$$

The *x*, *y* and *z* axes in the model correspond to the horizontal, vertical and transversal directions. The transversal direction is normal to the face of the walls and the vertical direction is parallel to the axis of the pillars. The total strain in each of the three directions and the three resulting planes depends on the type of cell.

The cuboid parts are designated by a set of initials. Throughout all the cases these are: *u* for units in general, *s* and *d* for stretcher and header units respectively where both are present (such as the Flemish bond case), *h* for head joints, *c* for cross joints, *b* for bed joints and *t* for transversal joints. Infill is designated as *i*. Dimensions are designated according to their orientation: *l* corresponds to a horizontal length, *h* to a vertical height and *t* to a transversal thickness. The dimension symbols are finally suffixed *u, m* or *i* for units, mortar and infill respectively, meaning that h_u is the unit height, h_m is the thickness of the bed joint, l_u is the unit length, l_m is the thickness of the head joint, t_u is the width of the unit, t_m is the thickness of the transversal joint and t_i is the transversal thickness of the infill.

Figure 4 illustrates the discretization of the single leaf wall cells along with the naming convention for each component in detail. The discretization of the multi leaf walls is shown in Figure 5 and that of the pillars in Figure 6.

Normal stress equilibrium equations are formed according to

$$\sum_n \sigma_{ii,n} A_n - \sigma_{ii} A = 0 \tag{7}$$

while shear stress equilibrium equations are formed according to

$$\sum_n \sigma_{ij,n} A_n - \sigma_{ij} A = 0 \tag{8}$$

where A is the total cross sectional area of the cell and A_n is the cross sectional area of cuboid n in direction i.

All normal and shear stress equilibriums at the faces or cross sections of the cell assure global equilibrium of internal and external stress. External stresses are averaged over the surface of the cell, meaning that there may exist a mismatch between the external average stress and the stress of an individual cuboid.

3.2 Stack Bond Wall

3.2.1 Cell Subjected to Normal Stress

Due to the simple geometrical layout of the cell, which does not include complex geometrical interlocking of mortar joints and units, shear stress components are disregarded for applied normal stress.

Normal strain conformity is assumed as follows:

$$\varepsilon_{zz,h} = \varepsilon_{zz,u} = \varepsilon_{zz,c} = \varepsilon_{zz,b}$$

$$\varepsilon_{xx,h} = \varepsilon_{xx,c}$$

$$\varepsilon_{xx,u} = \varepsilon_{xx,b} \tag{9}$$

$$\varepsilon_{yy,h} = \varepsilon_{yy,u}$$

$$\varepsilon_{yy,c} = \varepsilon_{yy,b}$$

The above strain conformity relations assume equal out-of-plane strains for all cuboids and equal in-plane strains for parallel cuboids in a given direction.

Horizontal normal stress equilibrium conditions at the right and left face of the cell are as follows:

$$\sigma_{xx}\left(h_u/2 + h_m/2\right) = \sigma_{xx,u}\, h_u/2 + \sigma_{xx,b}\, h_m/2 \tag{10}$$

$$\sigma_{xx}\left(h_u/2 + h_m/2\right) = \sigma_{xx,h}\, h_u/2 + \sigma_{xx,c}\, h_m/2$$

Vertical normal stress equilibrium conditions at the top and bottom faces of the cell are as follows:

$$\sigma_{yy}\left(l_m/2 + l_u/2\right) = \sigma_{yy,h}\, l_m/2 + \sigma_{yy,u}\, l_u/2 \tag{11}$$

$$\sigma_{yy}\left(l_m/2 + l_u/2\right) = \sigma_{yy,c}\, l_m/2 + \sigma_{yy,b}\, l_u/2$$

Transversal normal stress equilibrium at the front face of the cell is as follows:

$$\sigma_{zz}\left(l_m/2+l_u/2\right)\left(h_m/2+h_u/2\right)=$$
$$\sigma_{zz,h}\,l_m/2\cdot h_u/2+\sigma_{zz,u}\,l_u/2\cdot h_u/2+\sigma_{zz,c}\,l_m/2\cdot h_m/2+\sigma_{zz,b}\,l_u/2\cdot h_m/2 \tag{12}$$

The normal strains of the entire cell along the three axes can be calculated as

$$\varepsilon_{xx}=\left(\varepsilon_{xx,h}\,l_m/2+\varepsilon_{xx,u}\,l_u/2\right)\Big/\left(l_m/2+l_u/2\right)$$

$$\varepsilon_{yy}=\left(\varepsilon_{yy,h}\,h_u/2+\varepsilon_{yy,c}\,h_m/2\right)\Big/\left(h_u/2+h_m/2\right) \tag{13}$$

$$\varepsilon_{zz}=\varepsilon_{zz,h}$$

3.2.2 Cell Subjected to Shear Stress

For *xy* shear it is assumed that

$$\varepsilon_{xy,h}=\varepsilon_{xy,u} \tag{14}$$

$$\varepsilon_{xy,c}=\varepsilon_{xy,b}$$

The shear stress equilibrium conditions at the top and right faces of the cell are as follows:

$$\sigma_{xy}\left(l_m/2+l_u/2\right)=\sigma_{xy,h}\,l_m/2+\sigma_{xy,u}\,l_u/2$$

$$\sigma_{xy}\left(h_u/2+h_m/2\right)=\sigma_{xy,u}\,h_u/2+\sigma_{xy,b}\,h_m/2 \tag{15}$$

The cell shear strain can be calculated as

$$\varepsilon_{xy}=\left(\varepsilon_{xy,c}\,h_m/2+\varepsilon_{xy,h}\,h_u/2\right)\Big/\left(h_m/2+h_u/2\right) \tag{16}$$

For *xz* shear it is assumed that

$$\varepsilon_{xz,u}=\varepsilon_{xz,b}$$

$$\sigma_{xz,c}=\sigma_{xz,h}=\sigma_{xz} \tag{17}$$

Shear stress equilibrium at the right face of the cell is as follows:

$$\sigma_{xz}\left(h_m/2+h_u/2\right)=\sigma_{xz,b}\,h_m/2+\sigma_{xz,u}\,h_u/2 \tag{18}$$

The cell shear strain is equal to

$$\varepsilon_{xz}=\left(\varepsilon_{xz,u}l_u/2+\varepsilon_{xz,h}\,l_m/2\right)\Big/\left(l_u/2+l_m/2\right) \tag{19}$$

For yz strain it is assumed that

$$\varepsilon_{yz,h}=\varepsilon_{yz,u}$$

$$\varepsilon_{yz,c}=\varepsilon_{yz,b} \tag{20}$$

Shear stress equilibrium at the front and top faces of the cell is as follows:

$$\begin{aligned}&\sigma_{yz}\left(l_m/2+l_u/2\right)\left(h_m/2+h_u/2\right)=\\&\sigma_{yz,h}\,l_m/2\cdot h_u/2+\sigma_{yz,u}\,l_u/2\cdot h_u/2+\sigma_{yz,c}\,l_m/2\cdot h_m/2+\sigma_{yz,b}\,l_u/2\cdot h_m/2\end{aligned} \tag{21}$$

$$\sigma_{yz}\left(l_m/2+l_u/2\right)=\sigma_{yz,h}\,l_m/2+\sigma_{yz,u}\,l_u/2$$

The cell shear strain is equal to:

$$\varepsilon_{yz}=\left(\varepsilon_{yz,u}\,h_u/2+\varepsilon_{yz,b}\,h_m/2\right)\Big/\left(h_u/2+h_m/2\right) \tag{22}$$

3.3 Running Bond Wall

3.3.1 Cell Subjected to Normal Stress

The geometrical interlocking of the units and the mortar requires that the in plane shear stresses be taken into account for normal stress loading conditions. Therefore, apart from the three components of normal stress for each cuboid component, the *xy* shear stress and strains also have been included for the formulation of the system of equations. In turn, the compatibility conditions take into account the shear deformation of the cuboids, primarily those of the bed and cross joints, for applied loads in the horizontal direction. The resulting shear stresses are negligible for loading in the vertical and transversal directions.

The horizontal normal stress equilibrium conditions at the left face and at a cross section across the middle of the cell are expressed as follows:

$$\sigma_{xx}\left(h_m+h_u\right)=\sigma_{xx,u2}\,h_u/2+\sigma_{xx,c}h_m+\sigma_{xx,h}\,h_u/2 \tag{23}$$

$$\sigma_{xx}\left(h_m+h_u\right)=\sigma_{xx,u1}\,h_u/2+\sigma_{xx,b}h_m+\sigma_{xx,u1}\,h_u/2$$

The vertical normal stress equilibrium conditions at the top face and at a cross section across the middle of the cell are as follows:

$$\sigma_{yy}\left(l_m/2+l_u/2\right)=\sigma_{yy,h}\,l_m/2+\sigma_{yy,u1}\left(l_u/2-l_m/2\right)+\sigma_{yy,u2}\,l_m/2 \tag{24}$$

$$\sigma_{yy}\left(l_m/2+l_u/2\right)=\sigma_{yy,c}\,l_m/2+\sigma_{yy,b}\left(l_u/2-l_m/2\right)+\sigma_{yy,c}\,l_m/2$$

The transversal normal stress equilibrium condition at the front face of the cell is as follows:

$$\begin{aligned}&\sigma_{zz}\left(h_m+h_u\right)\left(l_u/2+l_m/2\right)=\\&h_u\left(\sigma_{zz,h}\,l_m/2+\sigma_{zz,u1}\left(l_u/2-l_m/2\right)+\sigma_{zz,u2}\,l_m/2\right)+h_m\left(2\sigma_{zz,c}\,l_m/2+\sigma_{zz,b}\left(l_u/2-l_m/2\right)\right)\end{aligned} \tag{25}$$

The shear stress equilibrium conditions at the top face and at a cross section across the middle of the cell are as follows:

$$\sigma_{xy,h}\,l_m/2+\sigma_{xy,u1}\left(l_u/2-l_m/2\right)+\sigma_{xy,u2}\,l_m/2=0 \tag{26}$$

$$\sigma_{xy,c}\,l_m/2+\sigma_{xy,b}\left(l_u/2-l_m/2\right)+\sigma_{xy,c}\,l_m/2=0$$

Deformation compatibility of the cuboids, considering both normal and shear deformation along the horizontal axis and only normal deformation along the vertical and transversal axis, is as follows:

$$\varepsilon_{zz,h}=\varepsilon_{zz,u1}=\varepsilon_{zz,u2}=\varepsilon_{zz,c}=\varepsilon_{zz,b}$$

$$\varepsilon_{yy,h}=\varepsilon_{yy,u1}=\varepsilon_{yy,u2}$$

$$\varepsilon_{yy,c} = \varepsilon_{yy,b} \tag{27}$$

$$\varepsilon_{xx,h} = \varepsilon_{xx,c}$$

$$\varepsilon_{xx,u1} = \varepsilon_{xx,b}$$

$$\left(\varepsilon_{xx,h}\, l_m/2 + \varepsilon_{xx,u1}\left(l_u/2 - l_m/2\right) + \varepsilon_{xx,u2}\, l_m/2 + \left(\varepsilon_{xy,h} + \varepsilon_{xy,u1} + \varepsilon_{xy,u2}\right)h_u/4\right) =$$

$$\left(2\varepsilon_{xx,c}\, l_m/2 + \varepsilon_{xx,b}\left(l_u/2 - l_m/2\right) + \left(2\varepsilon_{xy,c} + \varepsilon_{xy,b}\right)h_m/2\right)$$

The following assumptions are made about the normal and shear stress distribution in the cell:

$$\sigma_{xx,u1} = \sigma_{xx,u2} \tag{28}$$

$$\sigma_{xy,u1} = \sigma_{xy,u2} = \sigma_{xy,h}$$

These assumptions, coupled with the global shear stress equations for the cell results in zero shear stresses for the units and head joint. They also result in identical horizontal effective stresses for the u_1 and u_2 cuboids, which represent the unit. This invalidates the partition of the unit into two parts, but the distinction is meaningful for non-linear analysis, where the two unit parts may sustain different degrees of damage.

The normal strains of the entire cell along the three axes are equal to

$$\varepsilon_{xx} = \left(\varepsilon_{xx,h}\, l_m/2 + \varepsilon_{xx,u1}\left(l_u/2 - l_m/2\right) + \varepsilon_{xx,u2}\, l_m/2 + \left(\varepsilon_{xy,h} + \varepsilon_{xy,u1} + \varepsilon_{xy,u2}\right)h_u/4\right)\Big/\left(l_m/2 + l_u/2\right)$$

$$\varepsilon_{yy} = \left(\varepsilon_{yy,h}\, h_u/2 + \varepsilon_{yy,c} h_m + \varepsilon_{yy,u2}\, h_u/2\right)\Big/\left(h_u + h_m\right) \tag{29}$$

$$\varepsilon_{zz} = \varepsilon_{zz,h}$$

3.3.2 Cell Subjected to Shear Stress

For *xy* shear it is assumed that

$$\varepsilon_{xy,h} = \varepsilon_{xy,u1} = \varepsilon_{xy,u2} \tag{30}$$

$$\varepsilon_{xy,c} = \varepsilon_{xy,b}$$

The shear stress equilibrium conditions at a horizontal cross section and a vertical cross section at the middle of the cell are as follows:

$$\sigma_{xy}\left(l_u/2 + l_m/2\right) = \sigma_{xy,c}\, l_m/2 + \sigma_{xy,b}\left(l_u/2 - l_m/2\right) + \sigma_{xy,c,}\, l_m/2 \tag{31}$$

$$\sigma_{xy}\left(h_u + h_m\right) = \sigma_{xy,u1}\, h_u/2 + \sigma_{xy,b} h_m + \sigma_{xy,u1}\, h_u/2$$

The cell shear strain is equal to

$$\varepsilon_{xy} = \left(\varepsilon_{xy,h}\, h_u/2 + \varepsilon_{xy,c} h_m + \varepsilon_{xy,u2}\, h_u/2\right)\Big/\left(h_u + h_m\right) \tag{32}$$

For *xz* shear it is assumed that

$$\varepsilon_{xz,u1} = \varepsilon_{xz,b}$$

$$\varepsilon_{xz,u1} = \varepsilon_{xz,u2} \tag{33}$$

$$\sigma_{xz,c} = \sigma_{xz,u2}$$

The stress equilibrium conditions at the front and left face and at a cross section at the center of the cell are as follows:

$$\sigma_{xz}\left(h_m + h_u\right)\left(l_u/2 + l_m/2\right) =$$
$$h_u\left(\sigma_{xz,h}\, l_m/2 + \sigma_{xz,u1}\left(l_u/2 - l_m/2\right) + \sigma_{xz,u2}\, l_m/2\right) + h_m\left(2\sigma_{xz,c}\, l_m/2 + \sigma_{xz,b}\left(l_u/2 - l_m/2\right)\right)$$

$$\sigma_{xz}\left(h_m + h_u\right) = \sigma_{xz,h}\, h_u/2 + \sigma_{xz,c} h_m + \sigma_{xz,u2}\, h_u/2 \tag{34}$$

$$\sigma_{xz}\left(h_m + h_u\right) = \sigma_{xz,u1}\, h_u/2 + \sigma_{xz,b} h_m + \sigma_{xz,u1}\, h_u/2$$

The cell shear strain is equal to

$$\varepsilon_{xz} = \left(\varepsilon_{xy,h}\, l_m/2 + \varepsilon_{xy,u1}\left(l_u/2 - l_m/2\right) + \varepsilon_{xy,u2}\, l_m/2\right)\Big/\left(l_u/2 + l_m/2\right) \tag{35}$$

For *yz* shear it is assumed that

$$\varepsilon_{yz,h} = \varepsilon_{yz,u1} = \varepsilon_{yz,u2} \tag{36}$$

$$\varepsilon_{yz,c} = \varepsilon_{yz,b}$$

Shear stress equilibriums at the top and front faces of the cell are as follows:

$$\sigma_{yz}\left(l_u/2 + l_m/2\right) = \sigma_{yz,h}\, l_m/2 + \sigma_{yz,u1}\left(l_u/2 - l_m/2\right) + \sigma_{yz,u2}\, l_m/2 \tag{37}$$

$$\sigma_{yz}\left(h_m + h_u\right)\left(l_u/2 + l_m/2\right) =$$
$$h_u\left(\sigma_{yz,h}\, l_m/2 + \sigma_{yz,u1}\left(l_u/2 - l_m/2\right) + \sigma_{yz,u2}\, l_m/2\right) + h_m\left(2\sigma_{yz,c}\, l_m/2 + \sigma_{yz,b}\left(l_u/2 - l_m/2\right)\right)$$

The cell shear strain is equal to

$$\varepsilon_{yz} = \left(\varepsilon_{yz,h}\, h_u/2 + \varepsilon_{yz,c} h_m + \varepsilon_{yz,u2}\, h_u/2\right)\Big/\left(h_u + h_m\right) \tag{38}$$

3.4 Flemish Bond Wall

3.4.1 Cell Subjected to Normal Stress

As in the running bond cell model, the in-plane shear deformation of the bed joint is taken into account for normal stress loading. The transfer of stress across the transversal joint is also taken into account without, however, considering the effects of shear stress in other planes. Also, as in the case of the running bond cell, shear stresses are negligible for vertical and transversal applied normal stress.

The horizontal normal stress equilibrium conditions at the left face and at two cross sections along the length of the cell are as follows:

$$\sigma_{xx}\left(h_u + h_m\right)\left(t_u + t_m/2\right) =$$
$$\left(\sigma_{xx,d1} h_u/2 + \sigma_{xx,b1} h_m + \sigma_{xx,s3} h_u/2\right) t_u + \left(\sigma_{xx,d2} h_u/2 + \sigma_{xx,c2} h_m + \sigma_{xx,t3} h_u/2\right) t_m/2$$

$$\sigma_{xx}\left(h_u + h_m\right)\left(t_u + t_m/2\right) =$$
$$\left(\sigma_{xx,h1} h_u/2 + \sigma_{xx,c1} h_m + \sigma_{xx,s2} h_u/2\right) t_u + \left(\sigma_{xx,h2} h_u/2 + \sigma_{xx,c3} h_m + \sigma_{xx,t2} h_u/2\right) t_m/2 \tag{39}$$

$$\sigma_{xx}\left(h_u+h_m\right)\left(t_u+t_m/2\right)=$$
$$\left(\sigma_{xx,s1}h_u/2+\sigma_{xx,b2}h_m+\sigma_{xx,s1}h_u/2\right)t_u+\left(\sigma_{xx,t1}h_u/2+\sigma_{xx,c4}h_m+\sigma_{xx,t1}h_u/2\right)t_m/2$$

The vertical normal stress equilibrium conditions at the top face and at a cross section across the middle of the cell are as follows:

$$\begin{aligned}&\sigma_{yy}\left(t_u+t_m/2\right)\left(t_u/2+l_m+l_u/2\right)=\\&\left(\sigma_{yy,d1}t_u/2+\sigma_{yy,h1}l_m+\sigma_{yy,s1}\left(l_u/2-l_m-t_u/2\right)+\sigma_{yy,s2}l_m+\sigma_{yy,s3}t_u/2\right)t_u+\\&\left(\sigma_{yy,d2}t_u/2+\sigma_{yy,h2}l_m+\sigma_{yy,t1}\left(l_u/2-l_m-t_u/2\right)+\sigma_{yy,t2}l_m+\sigma_{yy,t3}t_u/2\right)t_m/2\end{aligned}\qquad(40)$$

$$\begin{aligned}&\sigma_{yy}\left(t_u+t_m/2\right)\left(t_u/2+l_m+l_u/2\right)=\\&\left(\sigma_{yy,b1}t_u/2+\sigma_{yy,c1}l_m+\sigma_{yy,b2}\left(l_u/2-l_m-t_u/2\right)+\sigma_{yy,c1}l_m+\sigma_{yy,b1}t_u/2\right)t_u+\\&\left(\sigma_{yy,c2}t_u/2+\sigma_{yy,c3}l_m+\sigma_{yy,c4}\left(l_u/2-l_m-t_u/2\right)+\sigma_{yy,c3}l_m+\sigma_{yy,c2}t_u/2\right)t_m/2\end{aligned}$$

The transversal normal stress equilibrium conditions at the front face and at a cross section across the middle of the cell are as follows:

$$\begin{aligned}&\sigma_{zz}\left(h_u+h_m\right)\left(t_u/2+l_m+l_u/2\right)=\\&\left(\sigma_{zz,d1}t_u/2+\sigma_{zz,h1}l_m+\sigma_{zz,s1}\left(l_u/2-l_m-t_u/2\right)+\sigma_{zz,s2}l_m+\sigma_{zz,s3}t_u/2\right)h_u+\\&\left(\sigma_{zz,b1}t_u+2\sigma_{zz,c1}l_m+\sigma_{zz,b2}\left(l_u/2-l_m-t_u/2\right)\right)h_m\end{aligned}\qquad(41)$$

$$\begin{aligned}&\sigma_{zz}\left(h_u+h_m\right)\left(t_u/2+l_m+l_u/2\right)=\\&\left(\sigma_{zz,d2}t_u/2+\sigma_{zz,h2}l_m+\sigma_{zz,t1}\left(l_u/2-l_m-t_u/2\right)+\sigma_{zz,t2}l_m+\sigma_{zz,t3}t_u/2\right)h_u+\\&\left(\sigma_{zz,c2}t_u+2\sigma_{zz,c3}l_m+\sigma_{zz,c4}\left(l_u/2-l_m-t_u/2\right)\right)h_m\end{aligned}$$

The shear stress equilibrium conditions at the top face and at a vertical cross section across the middle of the cell are as follows:

$$\begin{aligned}&\left(\sigma_{xy,d1}t_u/2+\sigma_{xy,h1}l_m+\sigma_{xy,s1}\left(l_u/2-l_m-t_u/2\right)+\sigma_{xy,s2}l_m+\sigma_{xy,s3}t_u/2\right)t_u+\\&\left(\sigma_{xy,d2}t_u/2+\sigma_{xy,h2}l_m+\sigma_{xy,t1}\left(l_u/2-l_m-t_u/2\right)+\sigma_{xy,t2}l_m+\sigma_{xy,t3}t_u/2\right)t_m/2=0\end{aligned}\qquad(42)$$

$$\begin{aligned}&\left(\sigma_{xy,b1}t_u/2+\sigma_{xy,c1}l_m+\sigma_{xy,b2}\left(l_u/2-l_m-t_u/2\right)+\sigma_{xy,c1}l_m+\sigma_{xy,b1}t_u/2\right)t_u+\\&\left(\sigma_{xy,c2}t_u/2+\sigma_{xy,c3}l_m+\sigma_{xy,c4}\left(l_u/2-l_m-t_u/2\right)+\sigma_{xy,c3}l_m+\sigma_{xy,c2}t_u/2\right)t_m/2=0\end{aligned}$$

Deformation compatibility of the cuboids, considering both normal and shear deformation along the horizontal axis and only normal deformation along the vertical and transversal axes, is as follows:

$$\begin{aligned}&\varepsilon_{xx,d1}t_u/2+\varepsilon_{xx,h1}l_m+\varepsilon_{xx,s1}\left(l_u/2-l_m-t_u/2\right)+\varepsilon_{xx,s2}l_m+\varepsilon_{xx,s3}t_u/2+\\&\left(\varepsilon_{xy,d1}+\varepsilon_{xy,h1}+\varepsilon_{xy,s1}+\varepsilon_{xy,s2}+\varepsilon_{xy,s3}\right)h_u/4=\\&\varepsilon_{xx,d2}t_u/2+\varepsilon_{xx,h2}l_m+\varepsilon_{xx,t1}\left(l_u/2-l_m-t_u/2\right)+\varepsilon_{xx,t2}l_m+\varepsilon_{xx,t3}t_u/2+\\&\left(\varepsilon_{xy,d2}+\varepsilon_{xy,h2}+\varepsilon_{xy,t1}+\varepsilon_{xy,t2}+\varepsilon_{xy,t3}\right)h_u/4\end{aligned} \tag{43}$$

$$\begin{aligned}&\varepsilon_{xx,d1}t_u/2+\varepsilon_{xx,h1}l_m+\varepsilon_{xx,s1}\left(l_u/2-l_m-t_u/2\right)+\varepsilon_{xx,s2}l_m+\varepsilon_{xx,s3}t_u/2+\\&\left(\varepsilon_{xy,d1}+\varepsilon_{xy,h1}+\varepsilon_{xy,s1}+\varepsilon_{xy,s2}+\varepsilon_{xy,s3}\right)h_u/4=\\&\varepsilon_{xx,b1}t_u/2+\varepsilon_{xx,c1}l_m+\varepsilon_{xx,b2}\left(l_u/2-l_m-t_u/2\right)+\varepsilon_{xx,c1}l_m+\varepsilon_{xx,b1}t_u/2+\\&\left(\varepsilon_{xy,b1}+\varepsilon_{xy,c1}+\varepsilon_{xy,b2}+\varepsilon_{xy,c1}+\varepsilon_{xy,b1}\right)h_m/2\end{aligned}$$

$$\begin{aligned}&\varepsilon_{xx,d1}t_u/2+\varepsilon_{xx,h1}l_m+\varepsilon_{xx,s1}\left(l_u/2-l_m-t_u/2\right)+\varepsilon_{xx,s2}l_m+\varepsilon_{xx,s3}t_u/2+\\&\left(\varepsilon_{xy,d1}+\varepsilon_{xy,h1}+\varepsilon_{xy,s1}+\varepsilon_{xy,s2}+\varepsilon_{xy,s3}\right)h_u/4=\\&\varepsilon_{xx,c2}t_u/2+\varepsilon_{xx,c3}l_m+\varepsilon_{xx,c4}\left(l_u/2-l_m-t_u/2\right)+\varepsilon_{xx,c3}l_m+\varepsilon_{xx,c2}t_u/2+\\&\left(\varepsilon_{xy,c2}+\varepsilon_{xy,c3}+\varepsilon_{xy,c4}+\varepsilon_{xy,c3}+\varepsilon_{xy,c2}\right)h_m/2\end{aligned}$$

$$\varepsilon_{zz,d1}t_u+\varepsilon_{zz,d2}t_m/2=\varepsilon_{zz,b1}t_u+\varepsilon_{zz,c2}t_m/2$$

$$\varepsilon_{zz,d1}t_u+\varepsilon_{zz,d2}t_m/2=\varepsilon_{zz,s3}t_u+\varepsilon_{zz,t3}t_m/2$$

$$\varepsilon_{zz,d1}t_u+\varepsilon_{zz,d2}t_m/2=\varepsilon_{zz,h1}t_u+\varepsilon_{zz,h2}t_m/2$$

$$\varepsilon_{zz,d1}t_u+\varepsilon_{zz,d2}t_m/2=\varepsilon_{zz,c1}t_u+\varepsilon_{zz,c3}t_m/2$$

$$\varepsilon_{zz,d1}t_u+\varepsilon_{zz,d2}t_m/2=\varepsilon_{zz,s2}t_u+\varepsilon_{zz,t2}t_m/2$$

$$\varepsilon_{zz,d1}t_u+\varepsilon_{zz,d2}t_m/2=\varepsilon_{zz,s1}t_u+\varepsilon_{zz,t1}t_m/2$$

$$\varepsilon_{zz,d1}t_u+\varepsilon_{zz,d2}t_m/2=\varepsilon_{zz,b2}t_u+\varepsilon_{zz,c4}t_m/2$$

$$\varepsilon_{xx,b1}=\varepsilon_{xx,c2}=\varepsilon_{xx,d1}$$

$$\varepsilon_{xx,s3} = \varepsilon_{xx,t3}$$

$$\varepsilon_{xx,c1} = \varepsilon_{xx,c3} = \varepsilon_{xx,h1} = \varepsilon_{xx,h2}$$

$$\varepsilon_{xx,s2} = \varepsilon_{xx,t2}$$

$$\varepsilon_{xx,s1} = \varepsilon_{xx,t1} = \varepsilon_{xx,b2}$$

$$\varepsilon_{xx,b2} = \varepsilon_{xx,c4}$$

$$\varepsilon_{yy,d1} = \varepsilon_{yy,h1} = \varepsilon_{yy,s1} = \varepsilon_{yy,s2} = \varepsilon_{yy,s3} = \varepsilon_{yy,d2} = \varepsilon_{yy,h2} = \varepsilon_{yy,t1} = \varepsilon_{yy,t2} = \varepsilon_{yy,t3}$$

$$\varepsilon_{yy,b1} = \varepsilon_{yy,c1} = \varepsilon_{yy,b2} = \varepsilon_{yy,c2} = \varepsilon_{yy,c3} = \varepsilon_{yy,c4}$$

$$\varepsilon_{zz,s1} = \varepsilon_{zz,s2} = \varepsilon_{zz,s3}$$

$$\varepsilon_{zz,d1} = \varepsilon_{zz,h1}$$

$$\varepsilon_{xy,d1} = \varepsilon_{xy,d2}$$

$$\varepsilon_{xy,h1} = \varepsilon_{xy,h2}$$

$$\varepsilon_{xy,s1} = \varepsilon_{xy,t1}$$

$$\varepsilon_{xy,s2} = \varepsilon_{xy,t2}$$

$$\varepsilon_{xy,s3} = \varepsilon_{xy,t3}$$

$$\varepsilon_{xy,b1} = \varepsilon_{xy,c2}$$

$$\varepsilon_{xy,c1} = \varepsilon_{xy,c3}$$

The following assumptions are made about the normal stress distribution in the cell:

$$\sigma_{zz,c1} = \sigma_{zz,c3}$$

$$\sigma_{zz,b2} = \sigma_{zz,c4}$$

$$\sigma_{zz,d1} = \sigma_{zz,d2} \tag{44}$$

$$\sigma_{zz,s1} = \sigma_{zz,t1}$$

$$\sigma_{zz,s2} = \sigma_{zz,t2}$$

$$\sigma_{zz,s3} = \sigma_{zz,t3}$$

The above set of equations assumes that the transversal normal stress is equal for the cuboids of the two leaves of masonry, be they unit or mortar. They also, again, lead to equal effective transversal stresses in the different cuboids comprising a single header brick. Damaged stresses in non-linear analysis, however, are different. For the shear stresses it is assumed that

$$\sigma_{xy,s1} = \sigma_{xy,s2} = \sigma_{xy,s3} = \sigma_{xy,h1} = \sigma_{xy,d1} \tag{45}$$

$$\sigma_{xy,b1} = \sigma_{xy,b2}$$

The normal strains of the entire cell along the three axes are equal to:

$$\varepsilon_{xx} = \left(\begin{array}{l} \varepsilon_{xx,d1} t_u/2 + \varepsilon_{xx,h1} l_m + \varepsilon_{xx,s1}\left(l_u/2 - l_m - t_u/2\right) + \varepsilon_{xx,s2} l_m + \varepsilon_{xx,s3} t_u/2 + \\ \left(\varepsilon_{xy,d1} + \varepsilon_{xy,h1} + \varepsilon_{xy,s1} + \varepsilon_{xy,s2} + \varepsilon_{xy,s3}\right) h_u/4 \end{array} \right) \Big/ \left(l_u/2 + l_m + t_u/2\right)$$

$$\varepsilon_{yy} = \left(\varepsilon_{yy,d1} h_u/2 + \varepsilon_{yy,b1} h_m + \varepsilon_{yy,s3} h_u/2\right) \Big/ \left(h_u + h_m\right) \tag{46}$$

$$\varepsilon_{zz} = \left(\varepsilon_{zz,d1} t_u + \varepsilon_{zz,d2} t_m/2\right) \Big/ \left(t_u + t_m/2\right)$$

3.4.2 Cell Subjected to Shear Stress

For *xy* shear it is assumed that:

$$\varepsilon_{xy,d1} = \varepsilon_{xy,h1} = \varepsilon_{xy,s1} = \varepsilon_{xy,s2} = \varepsilon_{xy,s3} = \varepsilon_{xy,d2} = \varepsilon_{xy,h2} = \varepsilon_{xy,t1} = \varepsilon_{xy,t2} = \varepsilon_{xy,t3} \tag{47}$$

$$\varepsilon_{xy,b1} = \varepsilon_{xy,c1} = \varepsilon_{xy,b2} = \varepsilon_{xy,c2} = \varepsilon_{xy,c3} = \varepsilon_{xy,c4}$$

The shear stress equilibrium condition at the left face and at a cross-section along the mid height of the cell are as follows:

$$\begin{aligned}
&\sigma_{xy}\left(t_u + t_m/2\right)\left(h_u + h_m\right) = \\
&\left(\sigma_{xy,d1}\, h_u/2 + \sigma_{xy,b1} h_m + \sigma_{xy,s3}\, h_u/2\right)t_u + \left(\sigma_{xy,d2}\, h_u/2 + \sigma_{xy,c2} h_m + \sigma_{xy,t3}\, h_u/2\right)t_m/2
\end{aligned}$$

$$\begin{aligned}
&\sigma_{xy}\left(t_u + t_m/2\right)\left(l_u/2 + l_m + t_u/2\right) = \\
&\left(\sigma_{xy,b1}\, t_u/2 + \sigma_{xy,c1} l_m + \sigma_{xy,b2}\left(l_u/2 - l_m - t_u/2\right) + \sigma_{xy,c1} l_m + \sigma_{xy,b1}\, t_u/2\right)t_u + \\
&\left(\sigma_{xy,c2}\, t_u/2 + \sigma_{xy,c3} l_m + \sigma_{xy,c4}\left(l_u/2 - l_m - t_u/2\right) + \sigma_{xy,c3} l_m + \sigma_{xy,c2}\, t_u/2\right)t_m/2
\end{aligned} \tag{48}$$

The cell shear strain is equal to

$$\varepsilon_{xy} = \left(\varepsilon_{xy,d1}\, h_u/2 + \varepsilon_{xy,b1} h_m + \varepsilon_{xy,s3}\, h_u/2\right)\Big/\left(h_u + h_m\right) \tag{49}$$

For *xz* shear it is assumed that

$$\varepsilon_{xz,d1} = \varepsilon_{xz,s1} = \varepsilon_{xz,s2} = \varepsilon_{xz,s3} = \varepsilon_{xz,b1} = \varepsilon_{xz,c1} = \varepsilon_{xz,b2} \tag{50}$$

$$\varepsilon_{xz,\mathrm{h}2} = \varepsilon_{xz,t1} = \varepsilon_{xz,t2} = \varepsilon_{xz,t3} = \varepsilon_{xz,c2} = \varepsilon_{xz,c3} = \varepsilon_{xz,c4}$$

The shear stress equilibrium conditions at the front face, transversal section at the middle, the left face and a vertical section along the middle of the cell are as follows:

$$\begin{aligned}
&\sigma_{xz}\left(l_u/2 + l_m + t_u/2\right)\left(h_u/2 + h_m/2\right) = \\
&\left(\sigma_{xz,d1}\, t_u/2 + \sigma_{xz,h1} l_m + \sigma_{xz,s1}\left(l_u/2 - l_m - t_u/2\right) + \sigma_{xz,s2} l_m + \sigma_{xz,s3}\, t_u/2\right)h_u/2 + \\
&\left(\sigma_{xz,b1}\, t_u/2 + \sigma_{xz,c1} l_m + \sigma_{xz,b2}\left(l_u/2 - l_m - t_u/2\right) + \sigma_{xz,c1} l_m + \sigma_{xz,b1}\, t_u/2\right)h_m/2
\end{aligned}$$

$$\sigma_{xz}\left(l_u/2+l_m+t_u/2\right)\left(h_u/2+h_m/2\right)=$$
$$\left(\sigma_{xz,d2}\,t_u/2+\sigma_{xz,h2}l_m+\sigma_{xz,t1}\left(l_u/2-l_m-t_u/2\right)+\sigma_{xz,t2}l_m+\sigma_{xz,t3}\,t_u/2\right)h_u/2+ \quad (51)$$
$$\left(\sigma_{xz,c2}\,t_u/2+\sigma_{xz,c3}l_m+\sigma_{xz,c4}\left(l_u/2-l_m-t_u/2\right)+\sigma_{xz,c3}l_m+\sigma_{xz,c2}\,t_u/2\right)h_m/2$$

$$\sigma_{xz}\left(t_u+t_m/2\right)\left(h_u+h_m\right)=$$
$$\left(\sigma_{xz,d1}\,h_u/2+\sigma_{xz,b1}h_m+\sigma_{xz,s3}\,h_u/2\right)t_u+\left(\sigma_{xz,d2}\,h_u/2+\sigma_{xz,c2}h_m+\sigma_{xz,t3}\,h_u/2\right)t_m/2$$

$$\sigma_{xz}\left(t_u+t_m/2\right)\left(h_u+h_m\right)=$$
$$\left(\sigma_{xz,s1}\,h_u/2+\sigma_{xz,b2}h_m+\sigma_{xz,s1}\,h_u/2\right)t_u+\left(\sigma_{xz,t1}\,h_u/2+\sigma_{xz,c4}h_m+\sigma_{xz,t1}\,h_u/2\right)t_m/2$$

The cell shear strain is equal to:

$$\varepsilon_{xz}=\left(\varepsilon_{xz,d1}\,t_u/2+\varepsilon_{xz,h1}l_m+\varepsilon_{xz,s1}\left(l_u/2-l_m-t_u/2\right)+\varepsilon_{xz,s2}l_m+\varepsilon_{xz,s3}\,t_u/2\right)\Big/\left(l_u/2+l_m+t_u/2\right) \quad (52)$$

For *yz* shear it is assumed that:

$$\varepsilon_{yz,d1}=\varepsilon_{yz,h1}=\varepsilon_{yz,s1}=\varepsilon_{yz,s2}=\varepsilon_{yz,s3}=\varepsilon_{yz,d2}=\varepsilon_{yz,h2}=\varepsilon_{yz,t1}=\varepsilon_{yz,t2}=\varepsilon_{yz,t3} \quad (53)$$

$$\varepsilon_{yz,b1}=\varepsilon_{yz,c1}=\varepsilon_{yz,b2}=\varepsilon_{yz,c2}=\varepsilon_{yz,c3}=\varepsilon_{yz,c4}$$

The shear stress equilibrium conditions at the front face and a horizontal cross section at the middle of the cell follows:

$$\sigma_{yz}\left(l_u/2+l_m+t_u/2\right)\left(h_u/2+h_m/2\right)=$$
$$\left(\sigma_{yz,d1}\,t_u/2+\sigma_{yz,h1}l_m+\sigma_{yz,s1}\left(l_u/2-l_m-t_u/2\right)+\sigma_{yz,s2}l_m+\sigma_{yz,s3}\,t_u/2\right)h_u/2+ \quad (54)$$
$$\left(\sigma_{yz,b1}\,t_u/2+\sigma_{yz,c1}l_m+\sigma_{yz,b2}\left(l_u/2-l_m-t_u/2\right)+\sigma_{yz,c1}l_m+\sigma_{yz,b1}\,t_u/2\right)h_m/2$$

$$\sigma_{yz}\left(t_u+t_m/2\right)\left(t_u/2+l_m+l_u/2\right)=$$
$$\left(\sigma_{yz,b1}\,t_u/2+\sigma_{yz,c1}l_m+\sigma_{yz,b2}\left(l_u/2-l_m-t_u/2\right)+\sigma_{yz,c1}l_m+\sigma_{yz,b1}\,t_u/2\right)t_u+$$
$$\left(\sigma_{yz,c2}\,t_u/2+\sigma_{yz,c3}l_m+\sigma_{yz,c4}\left(l_u/2-l_m-t_u/2\right)+\sigma_{yz,c3}l_m+\sigma_{yz,c2}\,t_u/2\right)t_m/2$$

The cell shear strain is equal to

$$\varepsilon_{yz} = \left(\varepsilon_{yz,s3}\, h_u/2 + \varepsilon_{yz,b1} h_m + \varepsilon_{yz,d1}\, h_u/2\right) \Big/ \left(h_u + h_m\right) \tag{55}$$

3.5 Three Leaf Wall

3.5.1 Cell Subjected to Normal Stress

The three leaf-model retains the set of assumptions made for the running bond model, which still apply to the outer masonry leaf. A number of further assumptions are made for the infill and the stress equilibrium conditions are modified to accommodate the new geometrical entities.

The horizontal normal stress equilibrium conditions at the left face and at a cross section across the middle of the cell are as follows:

$$\begin{aligned} &\sigma_{xx}\left(h_m + h_u\right)\left(t_u + t_i/2\right) = \\ &\left(\sigma_{xx,u2}\, h_u/2 + \sigma_{xx,c} h_m + \sigma_{xx,h}\, h_u/2\right) t_u + \left(\sigma_{xx,i3}\, h_u/2 + \sigma_{xx,i4} h_m + \sigma_{xx,i1}\, h_u/2\right) t_i/2 \end{aligned} \tag{56}$$

$$\begin{aligned} &\sigma_{xx}\left(h_m + h_u\right)\left(t_u + t_i/2\right) = \\ &\left(\sigma_{xx,u1}\, h_u/2 + \sigma_{xx,b} h_m + \sigma_{xx,u1}\, h_u/2\right) t_u + \left(\sigma_{xx,i2}\, h_u/2 + \sigma_{xx,i5} h_m + \sigma_{xx,i2}\, h_u/2\right) t_i/2 \end{aligned}$$

The vertical normal stress equilibrium conditions at the top face and at a cross section across the middle of the cell are as follows:

$$\begin{aligned} &\sigma_{yy}\left(l_m/2 + l_u/2\right)\left(t_u + t_i/2\right) = \\ &\left(\sigma_{yy,h}\, l_m/2 + \sigma_{yy,u1}\left(l_u/2 - l_m/2\right) + \sigma_{yy,u2}\, l_m/2\right) t_u + \left(\sigma_{yy,i1}\, l_m/2 + \sigma_{yy,i2}\left(l_u/2 - l_m/2\right) + \sigma_{yy,i3}\, l_m/2\right) t_i/2 \end{aligned} \tag{57}$$

$$\begin{aligned} &\sigma_{yy}\left(l_m/2 + l_u/2\right)\left(t_u + t_i/2\right) = \\ &\left(\sigma_{yy,\mathrm{c}}\, l_m/2 + \sigma_{yy,\mathrm{b}}\left(l_u/2 - l_m/2\right) + \sigma_{yy,\mathrm{c}}\, l_m/2\right) t_u + \left(\sigma_{yy,i4}\, l_m/2 + \sigma_{yy,i5}\left(l_u/2 - l_m/2\right) + \sigma_{yy,i4}\, l_m/2\right) t_i/2 \end{aligned}$$

The transversal normal stress equilibrium conditions at the front and back faces of the cell are as follows:

$$\begin{aligned} &\sigma_{zz}\left(h_m + h_u\right)\left(l_u/2 + l_m/2\right) = \\ &h_u\left(\sigma_{zz,h}\, l_m/2 + \sigma_{zz,u1}\left(l_u/2 - l_m/2\right) + \sigma_{zz,u2}\, l_m/2\right) + h_m\left(2\sigma_{zz,c}\, l_m/2 + \sigma_{zz,b}\left(l_u/2 - l_m/2\right)\right) \end{aligned} \tag{58}$$

$$\begin{aligned} &\sigma_{zz}\left(h_m + h_u\right)\left(l_u/2 + l_m/2\right) = \\ &h_u\left(\sigma_{zz,i1}\, l_m/2 + \sigma_{zz,i2}\left(l_u/2 - l_m/2\right) + \sigma_{zz,i3}\, l_m/2\right) + h_m\left(2\sigma_{zz,i4}\, l_m/2 + \sigma_{zz,i5}\left(l_u/2 - l_m/2\right)\right) \end{aligned}$$

The shear equilibrium conditions at the left face, a vertical cross section of the cell and at the top face of the cell read:

$$\left(\sigma_{xy,u2}\, h_u/2+\sigma_{xy,c} h_m+\sigma_{xy,h}\, h_u/2\right)t_u+\left(\sigma_{xy,i3}\, h_u/2+\sigma_{xy,i4} h_m+\sigma_{xy,i1}\, h_u/2\right)t_i/2=0$$

$$\left(\sigma_{xy,u1}\, h_u/2+\sigma_{xy,b} h_m+\sigma_{xy,c}\, h_u/2\right)t_u+\left(\sigma_{xy,i2}\, h_u/2+\sigma_{xy,i5} h_m+\sigma_{xy,i2}\, h_u/2\right)t_i/2=0 \qquad (59)$$

Constant normal stress is assumed in the infill, so that

$$\sigma_{xx,i1}=\sigma_{xx,i2}=\sigma_{xx,i3}=\sigma_{xx,i4}=\sigma_{xx,i5}$$

$$\sigma_{yy,i1}=\sigma_{yy,i2}=\sigma_{yy,i3}=\sigma_{yy,i4}=\sigma_{yy,i5} \qquad (60)$$

$$\sigma_{zz,i1}=\sigma_{zz,i2}=\sigma_{zz,i3}=\sigma_{zz,i4}=\sigma_{zz,i5}$$

Zero in-plane shear is assumed in the infill, leading to

$$\sigma_{xy,i1}=\sigma_{xy,i2}=\sigma_{xy,i3}=\sigma_{xy,i4}=\sigma_{xy,i5}=0 \qquad (61)$$

Two additional displacement conformity equations are introduced to accommodate the deformation of the infill. They read:

$$\begin{aligned}&\left(\varepsilon_{xx,h}\, l_m/2+\varepsilon_{xx,u1}\left(l_u/2-l_m/2\right)+\varepsilon_{xx,u2}\, l_m/2+\left(\varepsilon_{xy,h}+\varepsilon_{xy,u1}+\varepsilon_{xy,u2}\right)h_u/4\right)=\\&\left(\varepsilon_{xx,i1}\, l_m/2+\varepsilon_{xx,i2}\left(l_u/2-l_m/2\right)+\varepsilon_{xx,i3}\, l_m/2+\left(\varepsilon_{xy,i1}+\varepsilon_{xy,i2}+\varepsilon_{xy,i3}\right)h_m/2\right)\end{aligned} \qquad (62)$$

$$\begin{aligned}&\left(\varepsilon_{xx,h}\, l_m/2+\varepsilon_{xx,u1}\left(l_u/2-l_m/2\right)+\varepsilon_{xx,u2}\, l_m/2+\left(\varepsilon_{xy,h}+\varepsilon_{xy,u1}+\varepsilon_{xy,u2}\right)h_u/4\right)=\\&\left(2\varepsilon_{xx,c}\, l_m/2+\varepsilon_{xx,b}\left(l_u/2-l_m/2\right)+\left(2\varepsilon_{xy,c}+\varepsilon_{xy,b}\right)h_m/2\right)\end{aligned}$$

The total cell strain in the horizontal and vertical direction remains the same. The strain in the transversal direction is now defined as:

$$\varepsilon_{zz} = \left(\varepsilon_{zz,h} t_u + \varepsilon_{zz,i2}\, t_i/2\right) \Big/ \left(t_u + t_i/2\right) \tag{63}$$

3.5.2 Cell Subjected to Shear Stress

For *xy* shear the same assumptions as for the running bond cell apply, although several additional assumptions are needed. Based on these assumptions the equilibrium equations are again adjusted.

Constant shear strain is assumed in the infill, so that

$$\sigma_{xy,i1} = \sigma_{xy,i2} = \sigma_{xy,i3} = \sigma_{xy,i4} = \sigma_{xy,i5} \tag{64}$$

The shear stress equilibrium conditions at the top face and at a horizontal cross-section across the middle of the cell are expressed as

$$\begin{aligned} &\sigma_{xy}\left(l_m/2 + l_u/2\right)\left(t_u + t_i/2\right) = \\ &\left(\sigma_{xy,h}\, l_m/2 + \sigma_{xy,u1}\left(l_u/2 - l_m/2\right) + \sigma_{xy,u2}\, l_m/2\right) t_u + \left(\sigma_{xy,i1}\, l_m/2 + \sigma_{xy,i2}\left(l_u/2 - l_m/2\right) + \sigma_{xy,i3}\, l_m/2\right) t_i/2 \end{aligned} \tag{65}$$

$$\begin{aligned} &\sigma_{xy}\left(l_m/2 + l_u/2\right)\left(t_u + t_i/2\right) = \\ &\left(\sigma_{xy,\mathrm{c}}\, l_m/2 + \sigma_{xy,\mathrm{b}}\left(l_u/2 - l_m/2\right) + \sigma_{xy,\mathrm{c}}\, l_m/2\right) t_u + \left(\sigma_{xy,i4}\, l_m/2 + \sigma_{xy,i5}\left(l_u/2 - l_m/2\right) + \sigma_{xy,i4}\, l_m/2\right) t_i/2 \end{aligned}$$

Deformation conformity is assumed between the leaves, leading to

$$\varepsilon_{xy,h1}\, h_u/2 + \varepsilon_{xy,c1} h_m + \varepsilon_{xy,u2}\, h_u/2 = \varepsilon_{xy,i1}\, h_u/2 + \varepsilon_{xy,i4} h_m + \varepsilon_{xy,i3}\, h_u/2 \tag{66}$$

For *xz* shear the deformation of the cell is dominated by the deformation of the infill. Therefore, the system of equations and the assumptions need to be adjusted.

The shear stress equilibrium conditions at the back of the cell and at a vertical cross-section at the middle of the cell are as follows:

$$\begin{aligned} &\sigma_{xz}\left(h_m + h_u\right)\left(l_u/2 + l_m/2\right) = \\ &h_u\left(\sigma_{xz,i1}\, l_m/2 + \sigma_{xz,i2}\left(l_u/2 - l_m/2\right) + \sigma_{xz,i3}\, l_m/2\right) + h_m\left(2\sigma_{xz,i4}\, l_m/2 + \sigma_{xz,i5}\left(l_u/2 - l_m/2\right)\right) \end{aligned}$$

$$\begin{aligned} &\sigma_{xz}\left(h_m + h_u\right)\left(t_u + t_i/2\right) = \\ &\left(\sigma_{xz,u1}\, h_u/2 + \sigma_{xz,b} h_m + \sigma_{xz,u1}\, h_u/2\right) t_u + \left(\sigma_{xz,i2}\, h_u/2 + \sigma_{xz,i5} h_m + \sigma_{xz,i2}\, h_u/2\right) t_i/2 \end{aligned} \tag{67}$$

The stress assumptions read:

$$\sigma_{xz,i1} = \sigma_{xz,i2} = \sigma_{xz,i3} = \sigma_{xz,i4} = \sigma_{xz,i5} \tag{68}$$

The strain assumptions read:

$$\varepsilon_{xz,h} = \varepsilon_{xz,u1} = \varepsilon_{xz,u2} = \varepsilon_{xz,c} = \varepsilon_{xz,\mathrm{b}} \tag{69}$$

The total strain of the cell is defined as:

$$\varepsilon_{xz} = \left(\varepsilon_{xz,h} t_u + \varepsilon_{xz,i1} t_i/2\right) \Big/ \left(t_u + t_i/2\right) \tag{70}$$

For *yz* shear the deformation of the cell is again dominated by the deformation of the infill when its elastic modulus is low. However, the deformation profile changes for higher values of the Young's modulus of the infill since in this case the deformation of the outer leaf becomes more significant. Overall, the deformation is still dominated by the different stiffness between the outer and inner leaves.

The stress equilibrium conditions at the top, a horizontal cross section at mid height and at the front of the cell are as follows:

$$\begin{aligned}
&\sigma_{yz}\left(l_m/2 + l_u/2\right)\left(t_u + t_i/2\right) = \\
&\left(\sigma_{yz,h}\, l_m/2 + \sigma_{yz,u1}\left(l_u/2 - l_m/2\right) + \sigma_{yz,u2}\, l_m/2\right) t_u + \left(\sigma_{yz,i1}\, l_m/2 + \sigma_{yz,i2}\left(l_u/2 - l_m/2\right) + \sigma_{yz,i3}\, l_m/2\right) t_i/2 \\
&\\
&\sigma_{yz}\left(l_m/2 + l_u/2\right)\left(t_u + t_i/2\right) = \\
&\left(\sigma_{yz,c}\, l_m/2 + \sigma_{yz,b}\left(l_u/2 - l_m/2\right) + \sigma_{yz,c}\, l_m/2\right) t_u + \left(\sigma_{yz,i4}\, l_m/2 + \sigma_{yz,i5}\left(l_u/2 - l_m/2\right) + \sigma_{yz,i4}\, l_m/2\right) t_i/2 \\
&\\
&\sigma_{yz}\left(h_m + h_u\right)\left(l_u/2 + l_m/2\right) = \\
&h_u\left(\sigma_{yz,h}\, l_m/2 + \sigma_{yz,u1}\left(l_u/2 - l_m/2\right) + \sigma_{yz,u2}\, l_m/2\right) + h_m\left(2\sigma_{yz,c}\, l_m/2 + \sigma_{yz,b}\left(l_u/2 - l_m/2\right)\right)
\end{aligned} \tag{71}$$

The stress assumptions read:

$$\sigma_{yz,i1} = \sigma_{yz,h}$$

$$\sigma_{yz,i2} = \sigma_{yz,u1}$$

$$\sigma_{yz,i3} = \sigma_{yz,u2} \tag{72}$$

$$\sigma_{yz,i4} = \sigma_{yz,c}$$

$$\sigma_{yz,i5} = \sigma_{yz,b}$$

Deformation conformity conditions read:

$$\varepsilon_{xz,h} t_u + \varepsilon_{xz,t1}\, t_i/2 = \varepsilon_{xz,u2} t_u + \varepsilon_{xz,t3}\, t_i/2$$

$$\varepsilon_{xz,h}\, h_u/2 + \varepsilon_{xz,c} h_m + \varepsilon_{xz,u2}\, h_u/2 = \varepsilon_{xz,u1}\, h_u/2 + \varepsilon_{xz,b} h_m + \varepsilon_{xz,u1}\, h_u/2 \tag{73}$$

Since deformation conformity is not rigidly imposed, the total strain of the cell is defined according to the geometrical average of the cuboids participating in the total deformation of the cell according to

$$\varepsilon_{yz} = \left(\begin{array}{l} \left(\varepsilon_{yz,h} t_u + \varepsilon_{yz,i1}\, t_i/2\right)\frac{l_m}{2} + \\ \left(\varepsilon_{yz,u1} t_u + \varepsilon_{yz,i2}\, t_i/2\right)\frac{l_u - l_m}{2} + \\ \left(\varepsilon_{yz,u2} t_u + \varepsilon_{yz,i3}\, t_i/2\right)\frac{l_m}{2} \end{array} \right) \frac{h_u}{2} + \left(\begin{array}{l} \left(\varepsilon_{yz,c} t_u + \varepsilon_{yz,i4}\, t_i/2\right) l_m + \\ \left(\varepsilon_{yz,b} t_u + \varepsilon_{yz,i5}\, t_i/2\right)\frac{l_u - l_m}{2} \end{array} \right) \frac{h_m}{2} \Bigg/ \left(l_u/2 + l_m/2\right)\left(h_u/2 + h_m/2\right)\left(t_u + t_i/2\right) \tag{74}$$

3.6 Stack Bond Pillar

For the stack bond pillar model the system of equations developed by Haller for vertical normal stress is used [22].

According to Haller [20], the horizontal and transversal deformation equality of the two components reads:

$$\varepsilon_{xx,u} = \varepsilon_{xx,b} \text{ and } \varepsilon_{zz,u} = \varepsilon_{zz,b} \tag{75}$$

The horizontal and transversal stress equilibrium reads:

$$\sigma_{xx}\left(h_m+h_u\right)=\sigma_{xx,u}h_u+\sigma_{xx,b}h_m \text{ and } \sigma_{zz}\left(h_m+h_u\right)=\sigma_{zz,u}h_u+\sigma_{zz,b}h_m \tag{76}$$

The vertical stress equilibrium demands that both components develop vertical stress equal to the external load according to

$$\sigma_{yy,u}=\sigma_{yy,b}=\sigma_{yy} \tag{77}$$

The total vertical strain of the cell is

$$\varepsilon_{yy}=\left(\varepsilon_{yy,u}\,h_u/2+\varepsilon_{yy,b}\,h_m/2\right)\Big/\left(h_u/2+h_m/2\right) \tag{78}$$

3.7 English Bond Pillar

Shear stresses in the components are disregarded for applied normal stress. Normal strain conformity in the cell is achieved by assuming

$$\varepsilon_{xx,u1}=\varepsilon_{xx,b1}=\varepsilon_{xx,u3}=\varepsilon_{xx,h2}=\varepsilon_{xx,c2}=\varepsilon_{xx,u4} \text{ and } \varepsilon_{xx,u2}=\varepsilon_{xx,c1}=\varepsilon_{xx,h1}=\varepsilon_{xx,c4}=\varepsilon_{xx,c3}=\varepsilon_{xx,c5}$$

$$\varepsilon_{yy,u3}=\varepsilon_{yy,h1}=\varepsilon_{yy,u4}=\varepsilon_{yy,c5}\,,\ \varepsilon_{yy,b1}=\varepsilon_{yy,c1}=\varepsilon_{yy,c2}\ =\varepsilon_{yy,c3} \text{ and } \varepsilon_{yy,u2}=\varepsilon_{yy,c4}=\varepsilon_{yy,u1}=\varepsilon_{yy,h2} \tag{79}$$

$$\varepsilon_{zz,u2}=\varepsilon_{zz,c1}=\varepsilon_{zz,h1}=\varepsilon_{zz,u1}=\varepsilon_{zz,b1}=\varepsilon_{zz,u3} \text{ and } \varepsilon_{zz,c4}=\varepsilon_{zz,c3}=\varepsilon_{zz,c5}=\varepsilon_{zz,h2}=\varepsilon_{zz,c2}=\varepsilon_{zz,u4}$$

Normal stress equilibrium in the horizontal, vertical and transversal directions is expressed as

$$\sigma_{xx}\left(h_u+h_m\right)\left(l_u/2\right)=$$
$$\left(\sigma_{xx,h1}\left(l_u/2-l_m/2\right)+\sigma_{xx,c5}\,t_m/2\right)h_u/2+\left(\sigma_{xx,c1}\left(l_u/2-l_m/2\right)+\sigma_{xx,c3}\,t_m/2\right)h_m+\left(\sigma_{xx,u2}\left(l_u/2-l_m/2\right)+\sigma_{xx,c4}t_m/2\right)h_u/2$$

$$\sigma_{xx}\left(h_u+h_m\right)\left(l_u/2\right)=$$
$$\left(\sigma_{xx,u3}\left(l_u/2-l_m/2\right)+\sigma_{xx,u4}\,t_m/2\right)h_u/2+\left(\sigma_{xx,b1}\left(l_u/2-l_m/2\right)+\sigma_{xx,c2}\,t_m/2\right)h_m+\left(\sigma_{xx,u1}\left(l_u/2-l_m/2\right)+\sigma_{xx,h2}t_m/2\right)h_u/2$$

$$\sigma_{yy}\left(l_u/2\right)\left(l_u/2\right)=\left(\sigma_{yy,u3}\left(l_u/2-l_m/2\right)+\sigma_{yy,h1}t_m/2\right)\left(l_u/2-l_m/2\right)+\left(\sigma_{yy,c5}\,l_m/2+\sigma_{yy,u4}\left(l_u/2-l_m/2\right)\right)t_m/2$$

$$\sigma_{yy}\left(l_u/2\right)\left(l_u/2\right)=\left(\sigma_{yy,b1}\left(l_u/2-l_m/2\right)+\sigma_{yy,c1}t_m/2\right)\left(l_u/2-l_m/2\right)+\left(\sigma_{yy,c3}\,l_m/2+\sigma_{yy,c2}\left(l_u/2-l_m/2\right)\right)t_m/2 \tag{80}$$

$$\sigma_{yy}\left(l_u/2\right)\left(l_u/2\right)=\left(\sigma_{yy,u1}\left(l_u/2-l_m/2\right)+\sigma_{yy,u2}t_m/2\right)\left(l_u/2-l_m/2\right)+\left(\sigma_{yy,c4}\,l_m/2+\sigma_{yy,h2}\left(l_u/2-l_m/2\right)\right)t_m/2$$

$$\sigma_{zz}(h_u+h_m)(l_u/2)=$$
$$\left(\sigma_{zz,u3}\left(l_u/2-l_m/2\right)+\sigma_{zz,h1}\,l_m/2\right)h_u/2+\left(\sigma_{zz,b1}\left(l_u/2-l_m/2\right)+\sigma_{zz,c1}\,l_m/2\right)h_m+\left(\sigma_{zz,u1}\left(l_u/2-l_m/2\right)+\sigma_{zz,u2}\,l_m/2\right)h_u/2$$

$$\sigma_{zz}(h_u+h_m)(l_u/2)=$$
$$\left(\sigma_{zz,u4}\left(l_u/2-l_m/2\right)+\sigma_{zz,c5}\,l_m/2\right)h_u/2+\left(\sigma_{zz,c2}\left(l_u/2-l_m/2\right)+\sigma_{zz,c3}\,l_m/2\right)h_m+\left(\sigma_{zz,h2}\left(l_u/2-l_m/2\right)+\sigma_{zz,c4}\,l_m/2\right)h_u/2$$

The total vertical strain of the cell is

$$\varepsilon_{yy}=\left(\varepsilon_{yy,u3}\,h_u/2+\varepsilon_{yy,b1}h_m+\varepsilon_{yy,u1}\,h_u/2\right)\Big/\left(h_u/2+h_m+h_u/2\right) \qquad (81)$$

3.8 Calculation

For linear elastic analysis the solution from which the elastic moduli of the cell are derived can be accomplished in a single analysis step by solving the linear system of equations derived from the above expressions. For the application of normal stress, the systems need to be solved for the unknown normal stresses and strains and shear stresses and strains, where the latter two are considered. For the application of shear stress, the systems need to be solved for the arising shear stresses and strains.

For normal stress loading, the unknowns include three normal stresses, three normal strains, one shear stress and one shear strain value for each cuboid. However, in the stack bond wall, the stack bond pillar and the English bond pillar models shear stress and strain unknowns are not included. In summary, for normal stress loading, the stack bond wall system, consisting of four cuboids, is solved for 24 unknowns, the running bond wall for 40 unknowns for its five cuboids, the Flemish bond wall for 128 unknowns for its sixteen cuboids and the three-leaf wall is solved for 80 unknowns arising from ten cuboids. The stack bond pillar has two cuboids and its system has 12 unknowns and the English bond pillar has twelve cuboids resulting in a system of 72 unknowns. For shear stress loading each cuboid has one shear stress and one shear strain unknown components. Therefore, the number of unknowns is: 8 for the stack bond wall, 10 for the running bond wall, 32 for the Flemish bond wall and 20 for the three-leaf wall model.

Overall, obtaining closed form expressions for the stresses and strains in the cuboids, as well as for the elastic moduli of the cells, under conditions of applied normal stress is extremely difficult even for the simple case of stack bond masonry. Expressions for the shear moduli of the cells are far easier to be obtained due to the much smaller number of unknowns. However, the linear systems of equations can be solved with very little effort using simple linear algebra or any basic symbolic math software.

4. Verification of the Model

The capacity of the model to predict the elastic properties of masonry cells under normal and shear loading is initially evaluated through a comparison with the results obtained from FE analyses. The meshes used for this verification are shown in Figure 7. Apart from the comparison between the results obtained from the proposed model and the FE analyses, it is desirable to compare the two approaches in terms of computational cost.

The masonry unit cell is supposed to represent a volume of masonry inside an extended composite continuum. Therefore, boundary conditions assuring displacement conformity and periodicity at the cell faces need to be applied. Stress distribution in the constituents of the composite is not uniform but rather depends on the relative elasticity parameters of the involved components. The imposed boundary conditions ensure that the distribution of stress in the components is based on strain and deformation compatibility under normal and shear loading.

Periodicity conditions for a cell shown in Figure 8a are imposed by tying the displacements of nodes in opposite faces of the FE model. The tyings can be described as keeping the distance between two pairs of nodes equal, specifying a number of controlling nodes: *p1*, *p2*, *p3*, *p4* and *p5*. These controlling nodes also serve to fully describe the deformations necessary for the derivation of the elastic properties of the cell. Therefore the displacement of a node in face *i2* or *j2* for the application of a normal stress in the *i* direction or a shear stress in the *ij* plane can be derived from the displacement of the node in the opposite face *i1* or *j1* and the displacement of node *p1*, *p2* and *p3* as follows:

$$d_{i2} = d_{i1} + d_{p2} - d_{p1} \tag{82}$$

$$d_{j2} = d_{j1} + d_{p3} - d_{p1} \tag{83}$$

where d_{p1}, d_{p2} and d_{p3} are the displacement vectors of nodes *p1*, *p2* and *p3* in the *ij* plane and d_{i1}, d_{i2}, d_{j1} and d_{j2} are the displacement vectors of a node in faces *i1*, *i2*, *j1* and *j2* in the *ij* plane. Equal displacements in the *k* direction are imposed at the nodes of each of the external faces parallel to the *ij* plane for both applied normal and shear stress.

The elastic properties of the composite cell may be derived by registered displacements in the above designated controlling nodes, where $d_{pn,i}$ is equal to the displacement of node *n* in direction *i*. The total dimension of the cell in each principal direction *i* (horizontal, vertical and transversal) is designated as D_i. The Young's moduli and the Poisson's ratios of the cell may be calculated from

$$E_{c,i} = \sigma_{ii} / \varepsilon_{ii} = \sigma_{ii} \Big/ \left(\frac{d_i}{D_i} \right) = \sigma_{ii} \Big/ \left(\frac{d_{p2,i} - d_{p1,i}}{D_i} \right) \tag{84}$$

and

$$\begin{aligned} \nu_{c,ij} &= -\varepsilon_{jj} / \varepsilon_{ii} = -\left(\frac{d_j}{D_j} \right) \Big/ \left(\frac{d_i}{D_i} \right) = -\left(\frac{d_{p3,j} - d_{p1,j}}{D_j} \right) \Big/ \left(\frac{d_{p2,i} - d_{p1,i}}{D_i} \right) \\ \nu_{c,ik} &= -\varepsilon_{kk} / \varepsilon_{ii} = -\left(\frac{d_k}{D_k} \right) \Big/ \left(\frac{d_i}{D_i} \right) = -\left(\frac{d_{p5,k} - d_{p4,k}}{D_j} \right) \Big/ \left(\frac{d_{p2,i} - d_{p1,i}}{D_i} \right) \end{aligned} \tag{85}$$

where d_i, d_j and d_k are the relative displacements between two opposing faces in the *i*, *j* or *k* direction respectively, which can be expressed by the difference in displacement of opposing controlling nodes in a given direction.

The shear modulus of the cell is equal to

$$G_{c,ij} = \sigma_{ij} / 2\varepsilon_{ij} = \sigma_{ij} / \gamma_{ij} = \sigma_{ij} \Big/ \left(\frac{d_{p4,i} - d_{p1,i}}{D_j} + \frac{d_{p4,j} - d_{p1,j}}{D_i} \right) \tag{86}$$

The deformation profile of the cell under normal and shear applied stress is shown in Figure 8b and c.

A parametric investigation is conducted in order to verify the accuracy of the models for a wide range of ratios of unit-to-mortar and mortar-to-infill Young's modulus, as shown in Table 1. These properties and dimensions have been applied to all typologies of masonry under study. The parametric investigation of the three-leaf wall is conducted by assuming a ratio of 30 for the unit-to-mortar Young's modulus and altering the Young's modulus of the infill ranging from highly deformable to stiffer than the outer leaf. The wall models have been tested in all normal and shear directions and the pillar models have been tested for vertical loading.

Finally, a comparison is made between the results obtained by the model and experimental results drawn from the existing literature.

5. Results

5.1 Parametric Investigation

5.1.1 Overview

The analytical approach produced elastic results nearly identical to those obtained from FE analysis for all models and for almost the entire range of material properties. The Young's moduli and the Poisson's ratios of the masonry composites were calculated with great accuracy, with the differences being restricted to a number of shear moduli in out-off-plane loading.

The computational cost of the analytical models is negligible, the results being produced practically instantaneously on an ordinary computer, even for the largest systems of equations. The FE models required a computational time ranging from several seconds to a few minutes for the production of the results. The results of the parametric investigation and their comparison with FEM calculations are illustrated in Figure 9 through Figure 13.

The Young's moduli and Poisson's ratios for the stack bond case (Figure 9) are very well calculated. The shear moduli in the *xy* and *xz* planes are very similar due to the existence of the continuous bed mortar joint. The in-plane shear modulus is well approximated, while the two out-off-plane moduli are slightly overestimated by the model.

An interesting phenomenon is the tendency of the horizontal and vertical Young's moduli to be drastically reduced for a reduction of the Young's modulus of the mortar with the transversal modulus being reduced only slightly. For high values of the mortar modulus the three elastic moduli are of the same order of magnitude while for low values the transversal modulus is much higher. Certain conclusions may be drawn from this observation concerning the applicability of plane analysis methods for stack bond masonry structures. According to the relative deformability in the in-plane and out-of-plane directions, plane stress analysis may provide reasonable results for very rigid mortars and plane strain for very deformable mortars.

The vertical and transversal Young's modulus for running bond is almost exactly the same as for stack bond, but running bond has a higher horizontal modulus due to the staggered non-continuous layout of the horizontal joints, as illustrated in Figure 10. The model slightly underestimates the shear modulus in the *xz* plane for highly deformable mortars. Overall, the results are not drastically different from the ones obtained for stack bond masonry, although the accuracy of the model is slightly higher in the stack bond case.

Similar observations as those made for the relative deformability of the stack bond masonry in the in-plane and out-of-plane directions can be made for running bond masonry as well. The fact that both typologies are single leaf structures with constant geometry across the thickness of the cell indicate that this trend of the transversal Young's modulus of masonry to become much higher than the two in-plane ones may be shared by other singe leaf typologies. This assumption could be checked by further FEM or analytical calculations.

At this point a comparison may be here made between the proposed model and the model proposed by Zucchini & Lourenço [15] for running bond masonry. The models are nearly equally accurate for the prediction of the Young's modulus in all three orthogonal directions and the ν_{xy}, ν_{xz} and ν_{yz} Poisson's ratios: the average absolute error is 1.4% for the proposed model, with the maximum absolute error being 6%, while the Zucchini & Lourenço model has a 1.3% average and 6% maximum absolute error. For the prediction of the shear modulus the proposed model has an average absolute error of 3% and a maximum absolute error of 18%, which is registered for the G_{xz} modulus for $E_u/E_m = 1000$. The Zucchini & Lourenço model has a maximum error of only 5%, again for the G_{xz} modulus, which is registered for the G_{xz} modulus for $E_u/E_m = 10$. The reason for the reduced accuracy of the proposed model is the inclusion of shear stresses and strains only in the plane of the

applied external stress, whereas the Zucchini & Lourenço model includes shear stresses and strains in the *yz* plane in the bed joint.

In the Flemish bond wall case (Figure 11), due to the existence of the transversal joint, decreasing the Young's modulus of the mortar results in a decrease in the transversal Young's modulus of the cell. The discrepancy between the numerical and analytical results for the shear modulus in *xz* shear are similar to those in the previous cases, but all the remaining elastic properties are very well calculated.

The transversal joint eliminates the distinct higher rigidity in the transversal direction for highly deformable mortars noted in the stack bond and running bond typologies. However, the complex geometry across the thickness of the structure would render the plane stress and plane strain methods of analysis inappropriate by definition.

The model for the three-leaf wall case, whose results are shown in Figure 12, is capable of approximating the FEM results very well for the entire range of values. Of interest is the shift in the deformation profile of the cell under *yz* shear as the Young's modulus of the infill increases. For low values the obtained shear modulus is equal to the modulus in the *xz* plane and for higher values it is equal to the modulus in the *xy* plane. This is due to the deformability of the infill dominating the global response when highly deformable.

The horizontal and vertical Young's modulus and the in-plane shear modulus are only slightly affected by a reduction of the Young's modulus of the infill. The rest of the elastic moduli are greatly reduced. The infill influences the behavior of the masonry in a similar way to a continuous vertical or horizontal joint but in a transversal orientation.

The analytical models for the stack bond and English bond pillar, shown in Figure 13, produced results identical to the ones obtained from FE analyses. The deformation of the bed joint under vertical loading dominates the response in terms of global elastic stiffness and, as such, the existence of head and cross joints in the English bond pillar case has very small influence on the final results.

5.2 Case Studies

The modeling method has been applied to experimental cases consisting of stack bond, running bond and Flemish bond masonry composites found after an extensive literature review on masonry in compression [23–36]. Only case studies providing experimental values for the Young's modulus of the constituents have been considered. The cases and the analysis results are summarized in Table 2 through Table 5.The cases selected represent a wider range of material properties and dimensions that those considered in the parametric study. In a number of cases the Poisson's ratio is not given in the cited work and, therefore, a nominal value is used. In these cases, the value of the Poisson's ratio is indicated in brackets. The average value of the measured Poisson's ratio in the set of case studies is 0.15 with values ranging from 0.07 to 0.2. For the cases in which the value was unknown, a value was used based on the type of mortar used. Lower values were used for stronger mortars and higher values for weaker mortars in order to represent the lower deformability of the former and the higher deformability of the latter. In [23,31] a weak lime mortar was used, so a value of 0.25 is adopted. For [24,25,29,30,35], for which a cement/lime mortar was used, a value of 0.20 is adopted. In [33,34] Portland cement mortars were used and a value of 0.15 is used.

Again, the case studies have also been analyzed using FE models for the purpose of comparing the accuracy of the results and the computational cost.

The analytical model gives values nearly identical to the values obtained through FE analysis for the majority of the cases. The comparison with the experimental values shows significant agreement as well, especially for the stack bond pillar and running bond wall cases. The results of the case studies are illustrated in Figure 14.

6. Conclusions

Methods for the derivation of elastic and inelastic properties of masonry composites using micro-modeling techniques for the analysis of masonry periodic unit cells are presented and tested against results obtained from the analysis of corresponding FE cells and experimental results.

The results on the elastic properties of several types of masonry composites for a wide range of material combinations are well approximated using an analytical model based on simple calculations. Using FE

calculations as a benchmark, the elastic anisotropic behavior of masonry due to the interaction of isotropic components arranged in various typologies in a periodic structure is well simulated. Additionally, the comparison between the results of the proposed model and the available experimental results is fair.

Finally, the use of analytical models is shown to be very advantageous compared to FE calculations in terms of computational cost and model preparation time. The means required to implement the models for the derivation of the elastic properties of masonry only include simple linear algebra software.

The extension of the modelling technique herein presented for the nonlinear analysis of masonry walls and the prediction of their nonlinear properties will be presented in a following paper.

Acknowledgments

This research has received the financial support from the *Ministerio de Educación y Ciencia* through the research project SUBTIS (*Study of the Sensitivity of Urban Buildings to Tunneling Induced Settlements*, ref. num. BIA2009-13233), the project MICROPAR (*Identification of mechanical and strength parameter of structural masonry by experimental methods and numerical micro*-modeling, ref num. BIA2012-32234) and the ERDF (*European Regional Development Fund*).

Notation

E_u	Young's modulus of units
E_m	Young's modulus of mortar
E_i	Young's modulus of infill
$E_{c,i}$	Young's modulus of masonry in direction *i*
G_u	Shear modulus of units
$G_{c,ij}$	Shear modulus of masonry in plane *ij*

ν_u	Poisson's ratio of units
ν_m	Poisson's ratio of mortar
ν_i	Poisson's ratio of infill
$\nu_{c,ij}$	Poisson's ratio of masonry: contraction in direction *j* for applied extension in direction *i*
σ_{ii}	Normal stress in direction i
σ_{ij}	Shear stress in plane *ij*
h_u	Height of units
l_u	Length of units
t_u	Width of units
h_m	Thickness of mortar bed joint
l_m	Thickness of mortar head joint
t_m	Thickness of transversal mortar joint
t_i	Transversal thickness of infill
D_i	Dimension of cell in direction *i*
d_i	Deformation of cell in direction *i*
d_{pn}	Displacement vector of node *n*
$d_{pn,i}$	Displacement of node *n* in direction *i*

d_i^{ij} Deformation of cuboid in direction *i* due to shear strain in plane *ij*

References

[1] Anthoine A. Derivation of the in-plane elastic characteristics of masonry through homogenization theory. Int J Solids Struct 1995;32:137–63.

[2] Briccoli Bati S, Ranocchiai G, Rovero L. Suitability of micromechanical model for elastic analysis of masonry. J Eng Mech 1999;125:922–9.

[3] Cecchi A, Sab K. A multi-parameter homogenization study for modeling elastic masonry. Eur J Mech - A/Solids 2002;21:249–68.

[4] Lopez J, Oller S, Oñate E, Lubliner J. A Homogeneous Constitutive Model for Masonry. Int J Numer Methods Eng 1999;46:1651–71.

[5] Sacco E. A nonlinear homogenization procedure for periodic masonry. Eur J Mech A/Solids 2009;28:209–22.

[6] Milani G, Lourenço PB, Tralli A. Homogenised limit analysis of masonry walls, Part I: Failure surfaces. Comput Struct 2006;84:166–80.

[7] Cavalagli N, Cluni F, Gusella V. Strength domain of non-periodic masonry by homogenization in generalized plane state. Eur J Mech - A/Solids 2011;30:113–26.

[8] Massart TJ, Peerlings RHJ, Geers MGD, Gottcheiner S. Mesoscopic modeling of failure in brick masonry accounting for three-dimensional effects. Eng Fract Mech 2005;72:1238–53.

[9] Cluni F, Gusella V. Homogenization of non-periodic masonry structures. Int J Solids Struct 2004;41:1911–23.

[10] Pande G, Liang J, Middleton J. Equivalent elastic moduli for brick masonry. Comput Geotech 1989;8:243–65.

[11] Briccoli Bati S, Ranocchiai G, Rovero L. A micromechanical model for linear homogenization of brick masonry. Mater Struct 1999;32:22–30.

[12] Massart TJ, Peerlings RHJ, Geers MGD. Mesoscopic modeling of failure and damage-induced anisotropy in brick masonry. Eur J Mech - A/Solids 2004;23:719–35.

[13] Aboudi J. Mechanics of Composite Materials: A Unified Micromechanical Approach. Amsterdam: Studies in Applied Mechanics 29, Elsevier; 1991.

[14] Taliercio A. Closed-form expressions for the macroscopic in-plane elastic and creep coefficients of brick masonry. Int J Solids Struct 2014;51:2949–63.

[15] Zucchini A, Lourenço PB. A micro-mechanical model for the homogenisation of masonry. Int J Solids Struct 2002;39:3233–55.

[16] Addessi D, Sacco E. A kinematic enriched plane state formulation for the analysis of masonry panels. Eur J Mech A/Solids 2014;44:188–200.

[17] Zucchini A, Lourenço PB. A micro-mechanical homogenisation model for masonry: Application to shear walls. Int J Solids Struct 2009;46:871–86.

[18] Marfia S, Sacco E. Multiscale damage contact-friction model for periodic masonry walls. Comput Methods Appl Mech Eng 2012;205-208:189–203.

[19] Massart TJ, Peerlings RHJ, Geers MGD. An enhanced multi-scale approach for masonry wall computations with localization of damage. Int J Numer Methods Eng 2007;215089:1022–59.

[20] Milani G, Lourenço PB, Tralli A. Homogenised limit analysis of masonry walls, Part II: Structural examples. Comput Struct 2006;84:181–95.

[21] Addessi D, Sacco E. A multi-scale enriched model for the analysis of masonry panels. Int J Solids Struct 2012;49:865–80.

[22] Haller P. Hochhausbau in Backstein: die technische Eigenschaften von Backstein-Mauerwerk für Hochhäuser. Verband Schweiz. Ziegelindustrie VSZ; 1959.

[23] Drougkas A, Roca P, Molins C. Strength and elasticity of pure lime mortar masonry. Mater Struct 2015 (in press).

[24] Gumaste KS, Nanjunda Rao KS, Reddy BVV, Jagadish KS. Strength and elasticity of brick masonry prisms and wallettes under compression. Mater Struct 2007;40:241–53.

[25] Akbarzade A, Tasnimi A. Nonlinear Analysis and Modeling of Unreinforced Masonry Shear Walls Based on Plastic Damage Model. J Seismol Earthq Eng 2011;11:8–12.

[26] Schlegel R. Numerische Berechnung von Mauerwerkstrukturen in homogenen und diskreten Modellierungsstrategien. Bauhaus University, Weimar, Germany: PhD dissertation; 2004.

[27] Adam JM, Brencich A, Hughes TG, Jefferson T. Micromodelling of eccentrically loaded brickwork: Study of masonry wallettes. Eng Struct 2010;32:1244–51.

[28] Furtmüller T, Adam C. Numerical modeling of the in-plane behavior of historical brick masonry walls. Acta Mech 2011;221:65–77.

[29] Oliveira DV de C, Lourenço PB, Roca P. Cyclic behaviour of stone and brick masonry under uniaxial compressive loading. Mater Struct 2006;39:247–57.

[30] Vermeltfoort AT, Martens DRW, van Zijl GPAG. Brick–mortar interface effects on masonry under compression. Can J Civ Eng 2007;34:1475–85.

[31] Panizza M, Garbin E, Valluzzi MR, Modena C. Experimental investigation on bond of FRP/SRP applied to masonry prisms. 6th Int. Conf. FRP Compos. Civ. Eng. 2012, 2012, p. 13–5.

[32] Reddy BVV, Lal R, Nanjunda Rao KS. Influence of Joint Thickness and Mortar-Block Elastic Properties on the Strength and Stresses Developed in Soil-Cement Block Masonry. J Mater Civ Eng 2009;21:535–42.

[33] Kaushik HB, Rai DC, Jain SK. Stress-Strain Characteristics of Clay Brick Masonry under Uniaxial Compression. J Mater Civ Eng 2007:728–39.

[34] Hossain MM, Ali SS, Azadur Rahman M. Properties of Masonry Constituents. J Civ Eng Inst Eng Bangladesh 1997;CE 28:135–55.

[35] Page AW. Finite element model for masonry. J Struct Div ASCE 1978;104:1267–85.

[36] Binda L, Fontana A, G. Frigerio. Mechanical behaviour of brick masonries derived from unit and mortar characteristics. 8th Int. Brick Block Mason. Conf. Vol.1, Dublin, Irel., 1988, p. 205–16.

Figure Captions

Figure 1 Derivation of wall cells: full wall, repeating pattern and cell derived from geometrical symmetry of repeating pattern. (a) Stack bond wall, (b) running bond wall, (c) Flemish bond wall and (d) three-leaf wall with running bond outer leaf.

Figure 2 Derivation of pillar cells: full wall, repeating pattern and cell derived from geometrical symmetry of repeating pattern. (a) stack bond pillar and, (b) English bond pillar.

Figure 3 Discretization of periodic unit cells: (a) stack bond wall, (b) running bond wall, (c) Flemish bond wall, (d) three-leaf wall, (e) stack bond pillar and (f) English bond pillar.

Figure 4 Discretization and component designation of single leaf wall periodic unit cells: (a) stack bond and (b) running bond.

Figure 5 Discretization and component designation of multi leaf wall periodic unit cells: (a) Flemish bond and (b) three-leaf wall with running bond outer leaf.

Figure 6 Discretization and component designation of pillar periodic unit cells: (a) stack bond and (b) English bond.

Figure 7 Finite element models of wall periodic unit cells: (a) stack bond wall, (b) running bond wall, (c) Flemish bond wall, (d) three-leaf wall, (e) stack bond pillar and (f) English bond pillar cell.

Figure 8 **(a) FE model faces and nodes for definition of periodicity conditions. (b) Deformation profile of cell under uniaxial normal stress and (c) under pure shear stress.**

Figure 9 **Comparison between analytical model and numerical results for stack bond wall.**

Figure 10 **Comparison between analytical model and numerical results for running bond wall.**

Figure 11 **Comparison between analytical model and numerical results for Flemish bond wall.**

Figure 12 **Comparison between analytical model and numerical results for three-leaf wall with running bond exterior leaves.**

Figure 13 **Comparison between analytical model and numerical results for (a) stack bond pillar and (b) English bond pillar.**

Figure 14 **Comparison of vertical stiffness according to (a) FEM and analytical results and (b) experimental and analytical results. The dotted lines indicate the limits of 10% deviation between the compared values.**

Table Captions

Table 1 **Material properties and dimensions for linear elastic parametric analysis.**

Table 2 **Stack bond pillar cases: Comparison between experimental, FE and analytical results. Assumed values in curly brackets.**

Table 3 **Running bond wall cases: Comparison between experimental, FE and analytical results. Assumed values in curly brackets.**

Table 4 **Flemish bond wall cases: Comparison between experimental, FE and analytical results.**

Table 5 **English bond pillar cases: Comparison between experimental, FE and analytical results. Assumed values in curly brackets.**

Table 1

E_u [MPa]	v_u [-]	E_m [MPa]	v_m [-]	E_i [MPa]	v_i [-]	h_u [mm]	l_u [mm]	t_u [mm]	h_m [mm]	l_m [mm]	t_m [mm]	t_i [mm]
20000	0.15	20, 33, 67, 200, 333, 667, 2000, 3333, 6667, 20000	0.15	7, 11, 22, 67, 111, 222, 667, 2000, 4000, 6667	0.20	52	210	100	10	10	10	150

Table 2

Case	Ref.	E_u [MPa]	v_u [-]	h_u [mm]	l_u [mm]	t_u [mm]	E_m [MPa]	v_m [-]	h_m [mm]	l_m [mm]	t_m [mm]	$E_{c,\,exp}$ [MPa]	$E_{c,\,FEM}$ [MPa]	$E_{c,\,Analytical}$ [MPa]
S1	[23]	4200	0.16	45	290	140	125	{0.25}	10	-	-	729	814	705
S2	[24]	976	{0.15}	75	230	105	1500	{0.20}	12	-	-	467	1016	1025
S3	[24]	3372	{0.15}	75	230	105	8568	{0.20}	12	-	-	2393	3525	3692
S4	[25]	135	{0.15}	52	212	104	795	{0.20}	10	-	-	207	154	154
S5	[23]	4200	0.16	45	290	140	225	{0.25}	10	-	-	1181	1157	1138
S6	[26]	5500	0.11	113	240	175	2765	0.07	30	-	-	4200	4702	4555
S7	[24]	3372	{0.15}	75	230	105	5450	{0.20}	12	-	-	3135	3628	3560
S8	[24]	976	{0.15}	75	230	105	238	{0.20}	12	-	-	379	735	701
S9	[27]	2000	0.10	55	250	110	1700	0.20	10	-	-	1936	1950	1956
S10	[28]	7500	0.07	65	40	40	220	0.20	20	-	-	878	1475	937
S11	[29]	12000	0.20	45	285	130	4200	{0.20}	10	-	-	10000	9761	9110
S12	[26]	5500	0.11	238	252	241	2765	0.07	12	-	-	5517	5330	5250
S13	[30]	16700	0.15	52	210	100	2100	0.22	13	-	-	6800	8294	7486
S14	[31]	5756	{0.15}	55	125	120	5487	{0.25}	10	-	-	2132	5906	5736
S15	[24]	976	{0.15}	75	230	105	8568	{0.20}	12	-	-	365	1098	1137
S16	[32]	8000	0.08	100	305	143	6600	0.19	30	-	-	5900	7013	7687
S17	[28]	7500	0.07	65	40	40	220	0.20	10	-	-	1938	2380	1509
S18	24]	3372	{0.15}	75	230	105	7083	{0.20}	12	-	-	3700	3585	3641
S19	[33]	5300	{0.15}	75	230	110	545	{0.15}	10	-	-	2239	3034	2679
S20	[34]	12930	{0.15}	36	123	60	9590	{0.15}	7	-	-	8000	12601	12244

Table 3

Case	Ref.	E_u [MPa]	v_u [-]	h_u [mm]	l_u [mm]	t_u [mm]	E_m [MPa]	v_m [-]	h_m [mm]	l_m [mm]	t_m [mm]	$E_{c,\,exp}$ [MPa]	$E_{c,\,FEM}$ [MPa]	$E_{c,\,Analytical}$ [MPa]
R1	[24]	3372	{0.15}	75	230	105	5450	{0.20}	12	12	-	5232	3590	3660
R2	[30]	4000	0.13	50	206	96	1650	{0.20}	12.5	10	-	3200	3095	3114
R3	[24]	976	{0.15}	75	230	105	238	{0.20}	12	12	-	580	717	685
R4	[24]	976	{0.15}	75	230	105	1500	{0.20}	12	12	-	735	1033	1050
R5	[24]	3372	{0.15}	75	230	105	7083	{0.20}	12	12	-	4824	3702	3825
R6	[24]	3372	{0.15}	75	230	105	8568	{0.20}	12	12	-	5024	3782	3863
R7	[35]	6740	0.167	35	110	50	970	{0.20}	5	5	-	3700	3949	3936
R8	[24]	976	{0.15}	75	230	105	8568	{0.20}	12	12	-	400	1254	1561

Table 4

Case	Ref.	E_u [MPa]	v_u [-]	h_u [mm]	l_u [mm]	t_u [mm]	E_m [MPa]	v_m [-]	h_m [mm]	l_m [mm]	t_m [mm]	$E_{c,\,exp}$ [MPa]	$E_{c,\,FEM}$ [MPa]	$E_{c,\,Analytical}$ [MPa]
F1	[36]	4865	0.09	55	250	120	1180	0.06	10	10	10	1651	3107	3178
F2	[36]	4865	0.09	55	250	120	5650	0.09	10	10	10	3833	5002	5025
F3	[36]	4865	0.09	55	250	120	17760	0.12	10	10	10	4567	6390	6547

Table 5

Case	Ref.	E_u [MPa]	v_u [-]	h_u [mm]	l_u [mm]	t_u [mm]	E_m [MPa]	v_m [-]	h_m [mm]	l_m [mm]	t_m [mm]	$E_{c,\,exp}$ [MPa]	$E_{c,\,FEM}$ [MPa]	$E_{c,\,Analytical}$ [MPa]
P1	[24]	3372	{0.15}	75	230	105	8568	{0.20}	12	20	20	3317	4005	4157
P2	[24]	3372	{0.15}	75	230	105	5450	{0.20}	12	20	20	3789	3684	3736
P3	[24]	976	{0.15}	75	230	105	238	{0.20}	12	20	20	377	690	663
P4	[24]	3372	{0.15}	75	230	105	7083	{0.20}	12	20	20	3677	3865	3966
P5	[24]	976	{0.15}	75	230	105	1500	{0.20}	12	20	20	381	1056	1070
P6	[24]	976	{0.15}	75	230	105	8568	{0.20}	12	20	20	376	1510	1869
P7	[28]	7500	0.07	65	290	150	220	0.2	10	10	10	661	2007	1500

Figure 1

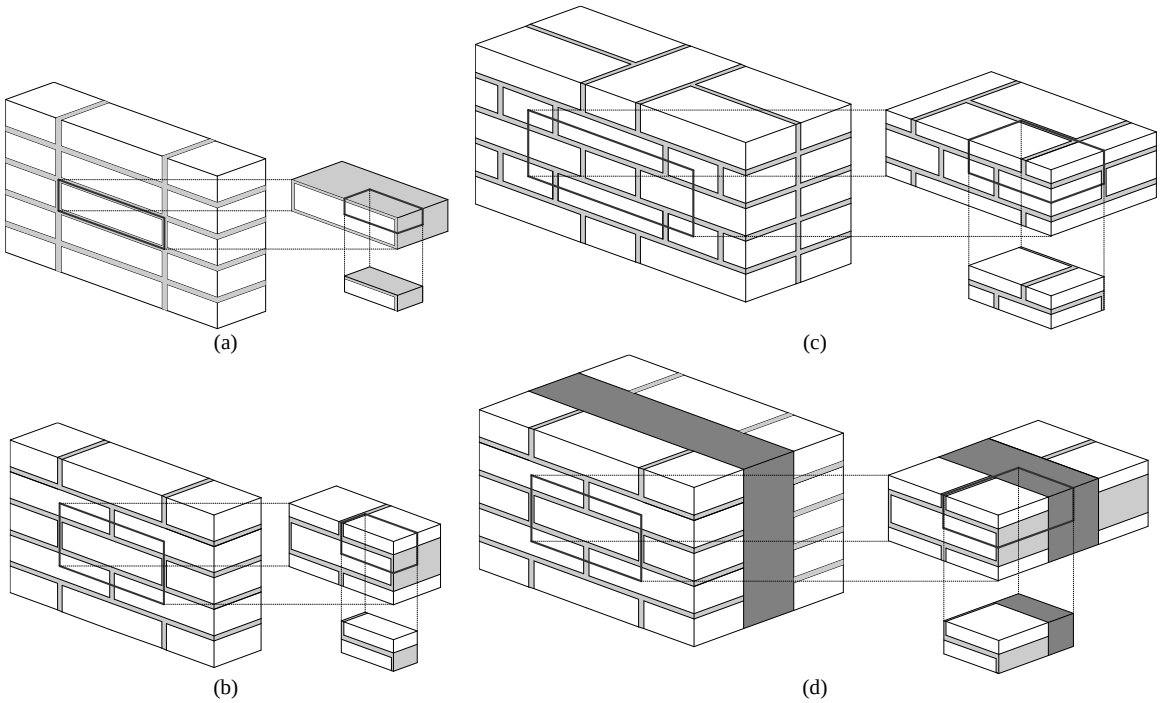

Figure 2

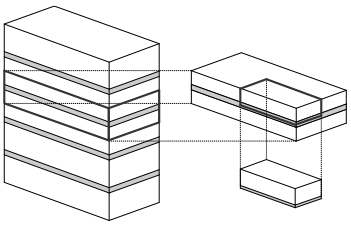

(a)

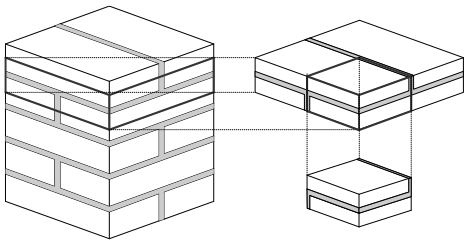

(b)

Figure 3

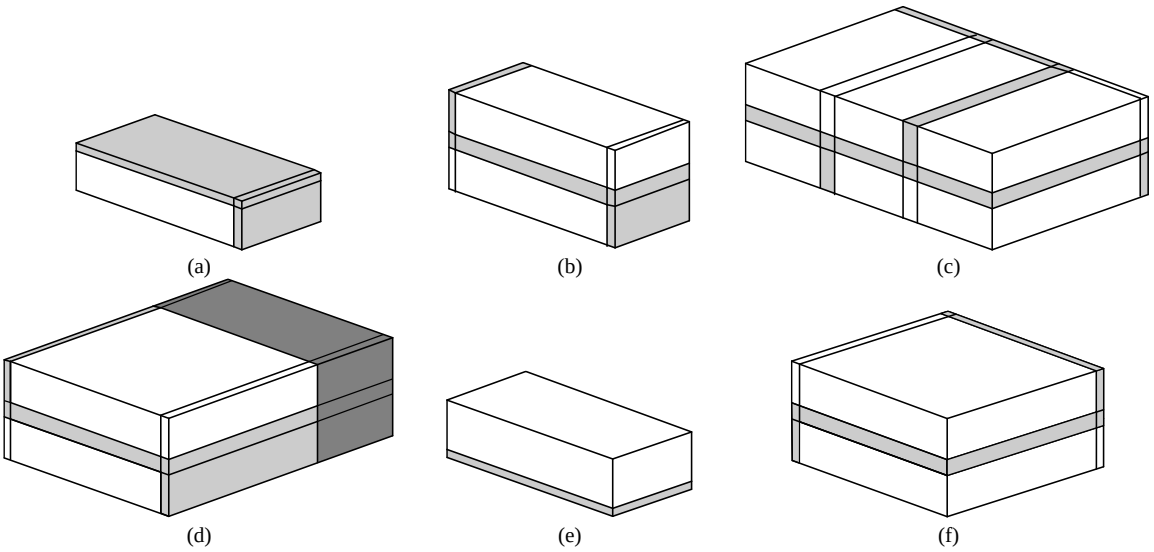

Figure 4

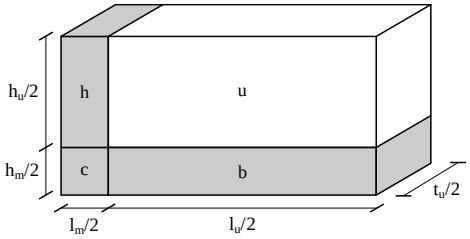
$h_u/2$
$h_m/2$
h
u
c
b
$t_u/2$
$l_m/2$
$l_u/2$

(a)

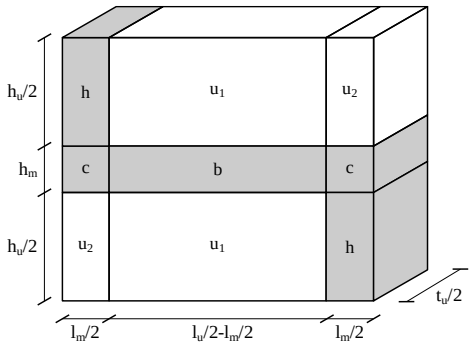
$h_u/2$
h_m
$h_u/2$
h
u_1
u_2
c
b
c
u_2
u_1
h
$t_u/2$
$l_m/2$
$l_u/2-l_m/2$
$l_m/2$

(b)

Figure 5

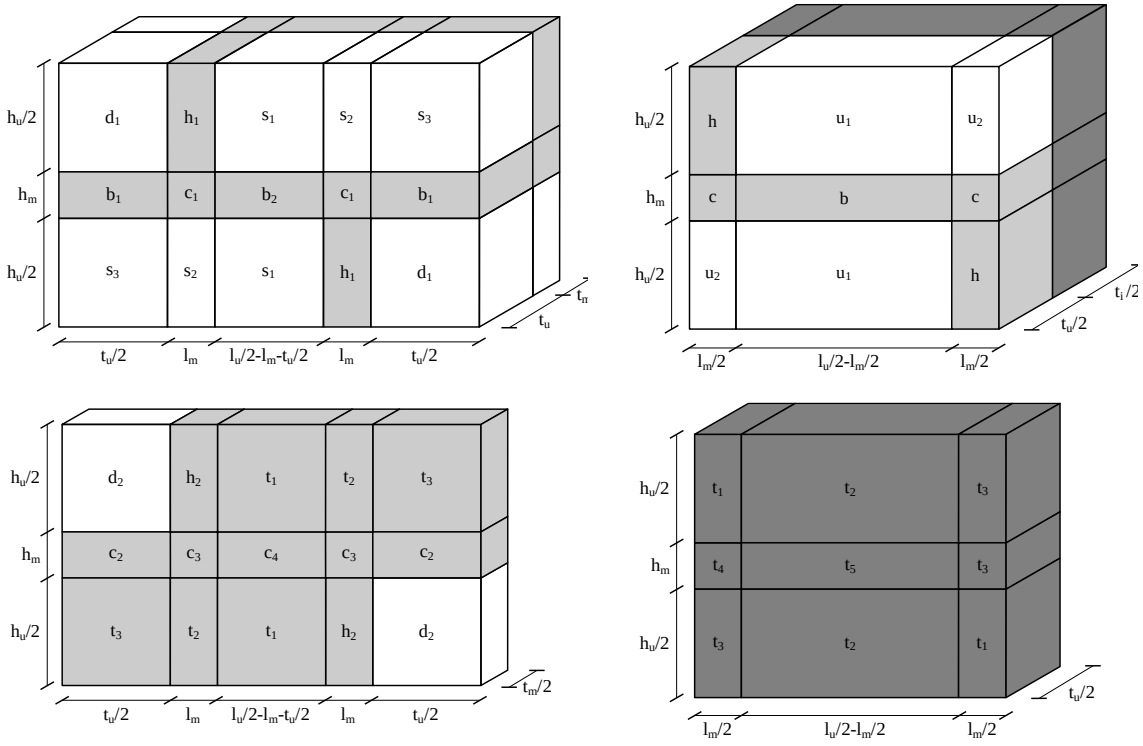
h_u/2
h_m
h_u/2
d_1
h_1
s_1
s_2
s_3
b_1
c_1
b_2
c_1
b_1
s_3
s_2
s_1
h_1
d_1
t_u/2
l_m
l_u/2-l_m-t_u/2
l_m
t_u/2
t_u
h
u_1
u_2
c
b
c
u_2
u_1
h
l_m/2
l_u/2-l_m/2
l_m/2
t_u/2
d_2
h_2
t_1
t_2
t_3
c_2
c_3
c_4
c_3
c_2
t_3
t_2
t_1
h_2
d_2
t_m/2
t_4
t_5

(a) (b)

Figure 6

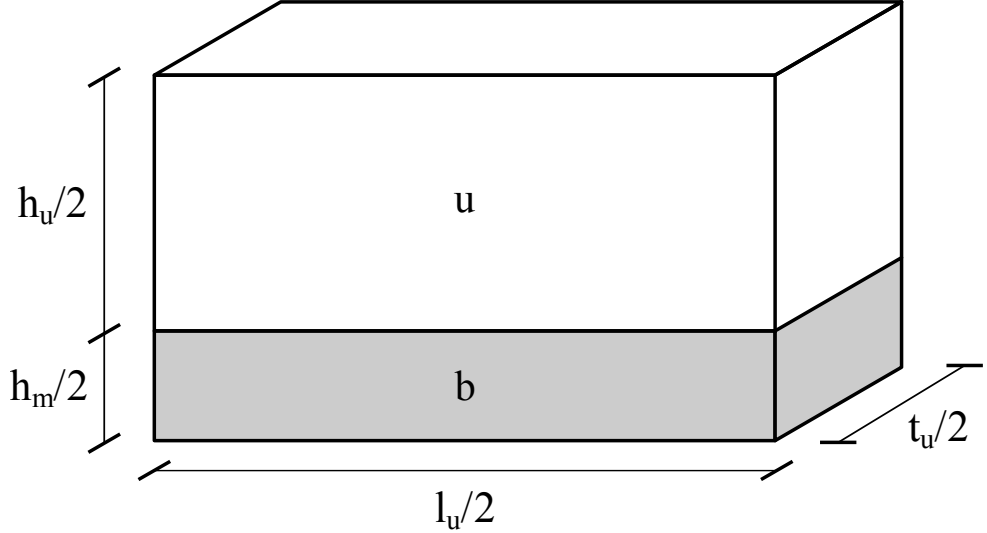
u
b
$h_u/2$
$h_m/2$
$t_u/2$
$l_u/2$

(a)

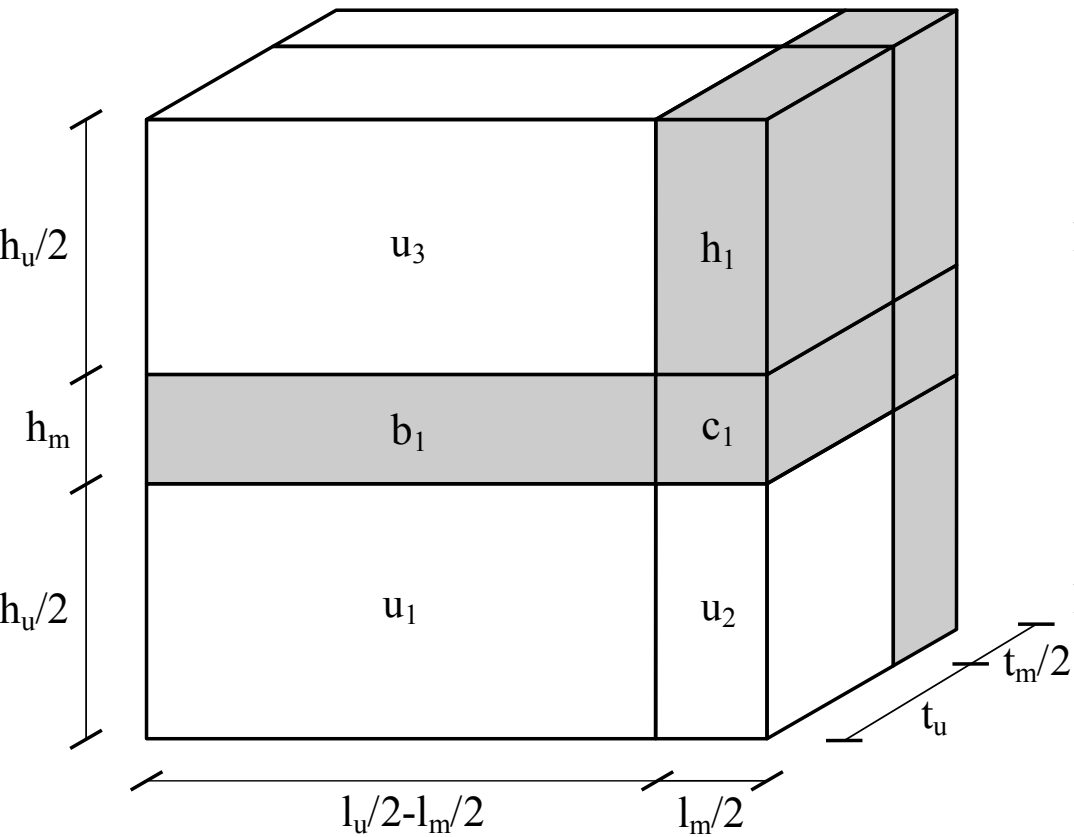
u_3
h_1
b_1
c_1
u_1
u_2
$h_u/2$
h_m
$h_u/2$
$t_m/2$
t_u
$l_u/2-l_m/2$
$l_m/2$

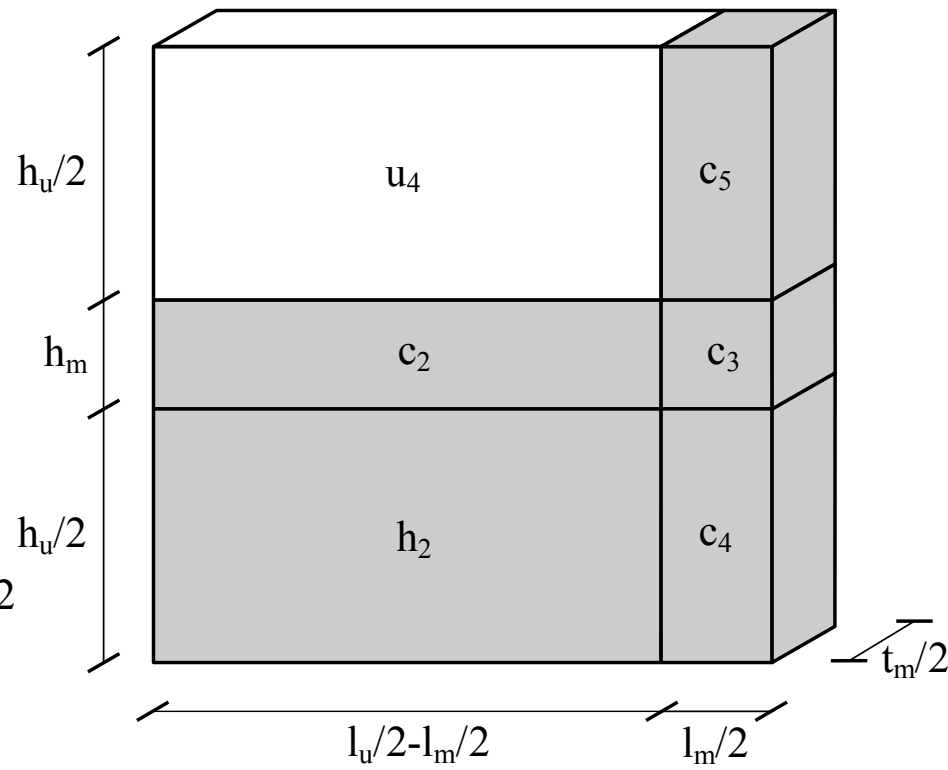
u_4
c_5
c_2
c_3
h_2
c_4
$h_u/2$
h_m
$h_u/2$
$t_m/2$
$l_u/2-l_m/2$
$l_m/2$

(b)

Figure 7

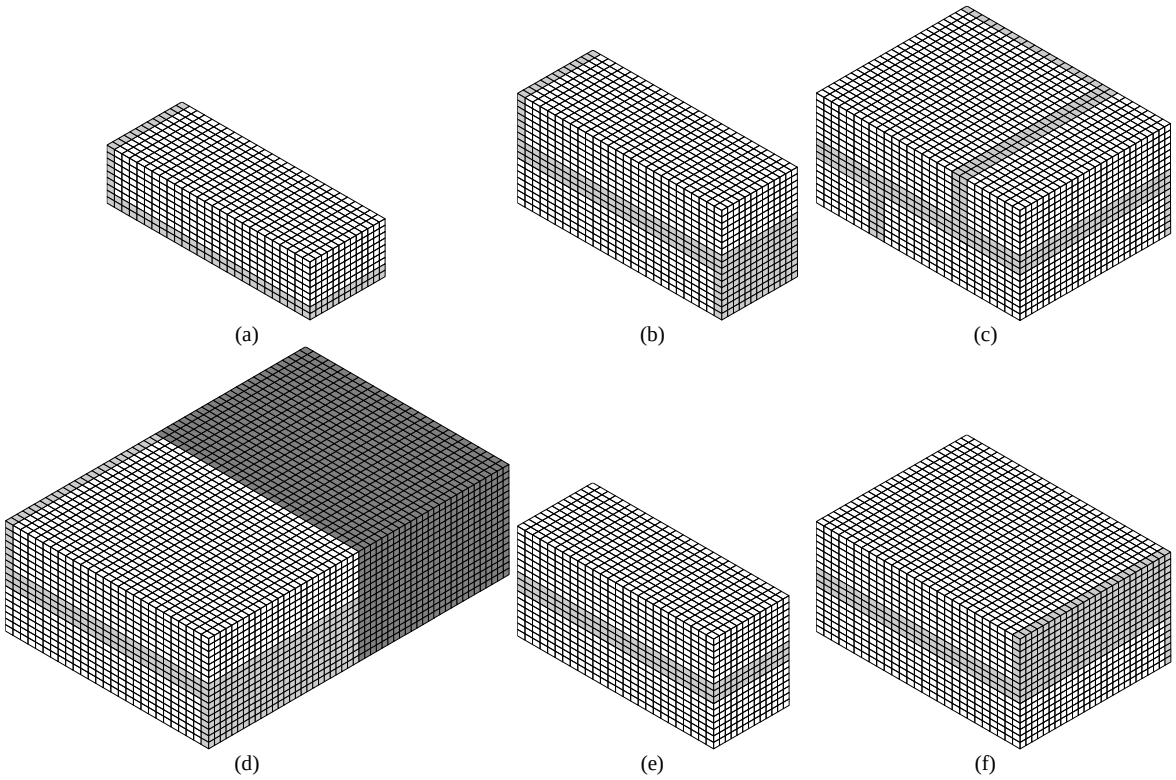

Figure 8

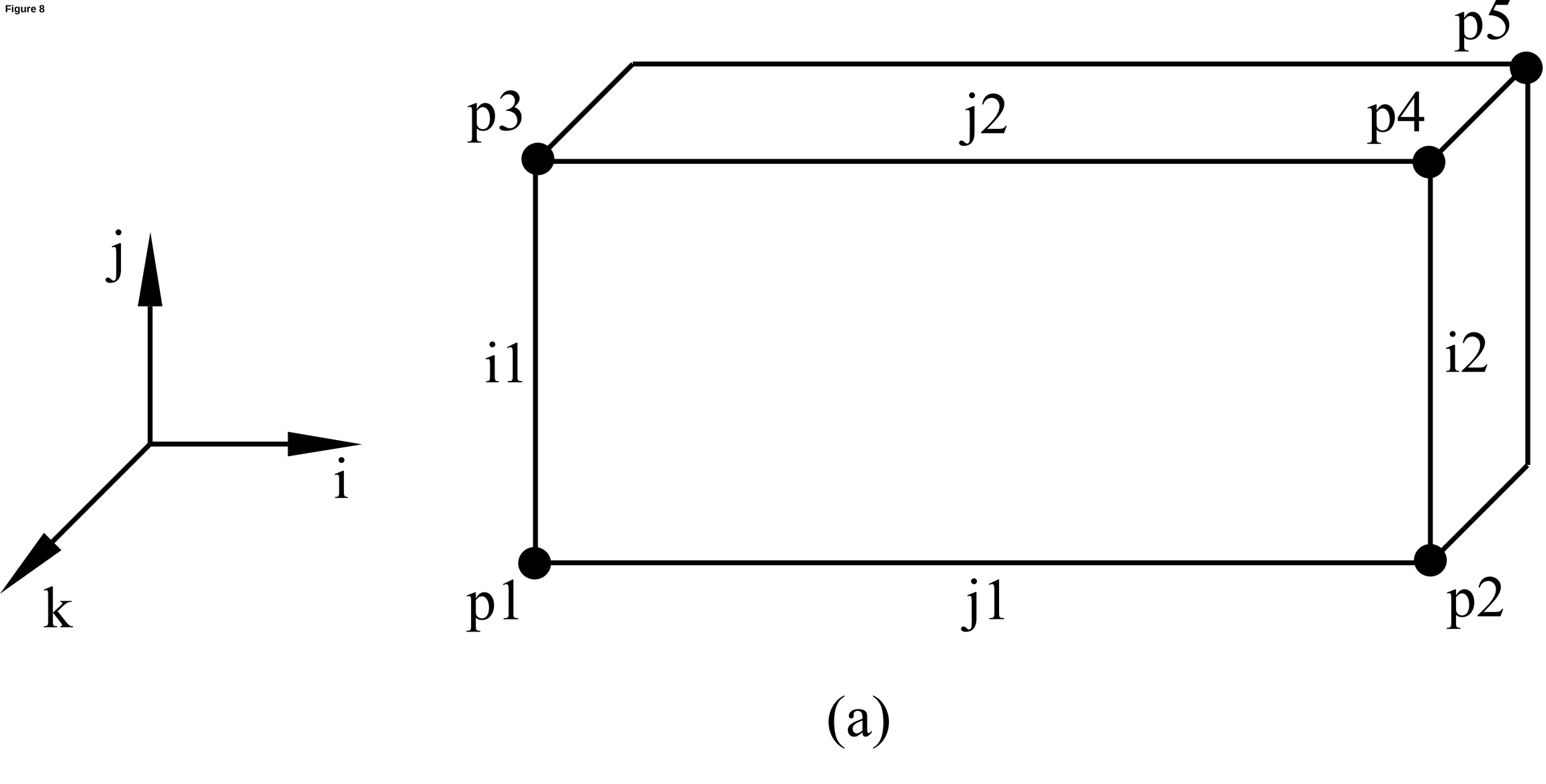

(a)

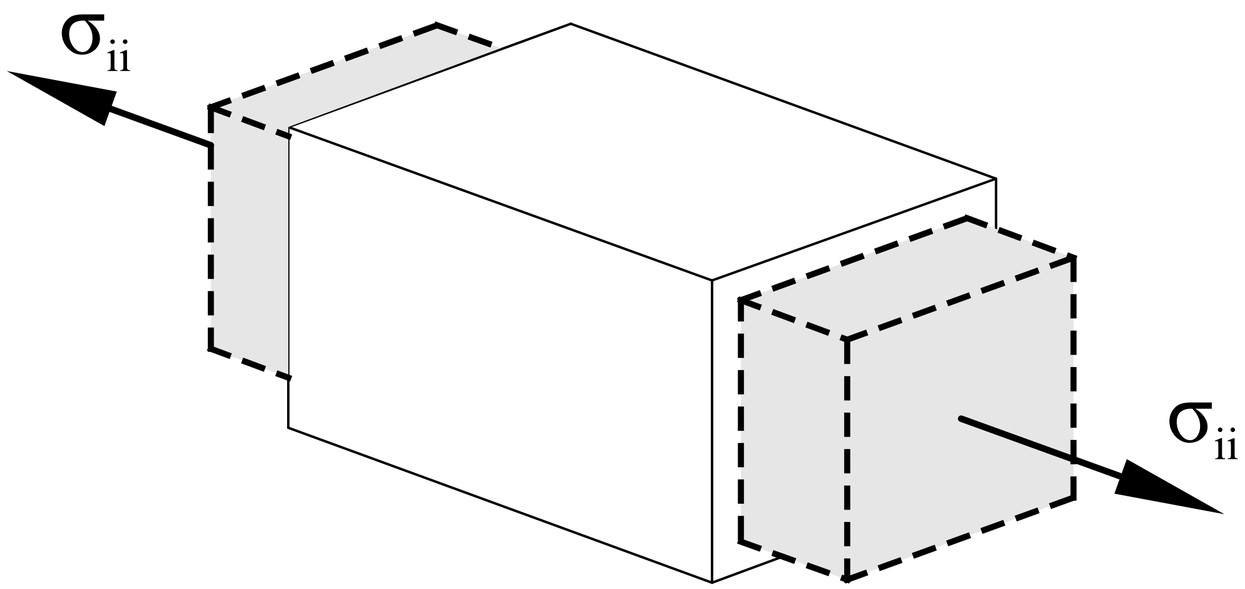

(b)

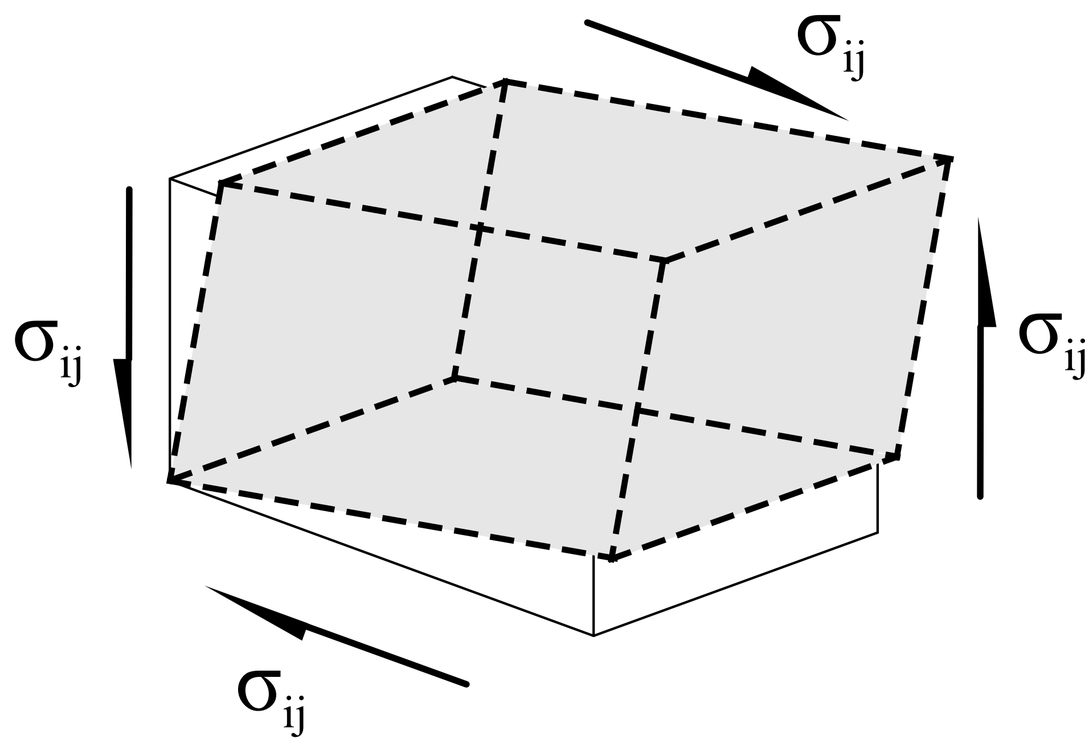

(c)

Figure 9

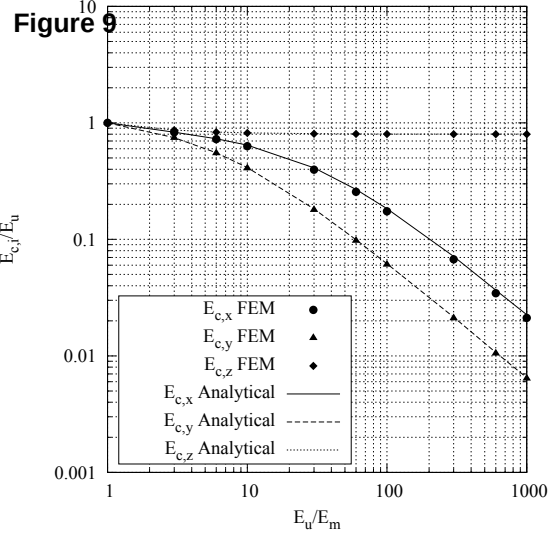
10
1
0.1
0.01
0.001
1
10
100
1000
$E_{c,i}/E_u$
E_u/E_m
$E_{c,x}$ FEM
$E_{c,y}$ FEM
$E_{c,z}$ FEM
$E_{c,x}$ Analytical
$E_{c,y}$ Analytical
$E_{c,z}$ Analytical

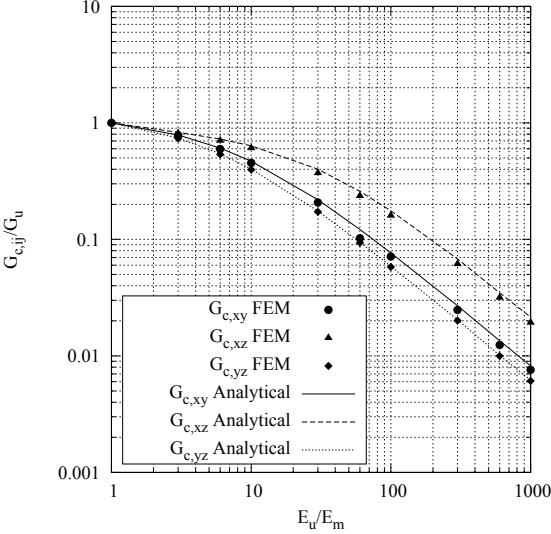
10
1
0.1
0.01
0.001
1
10
100
1000
$G_{c,ij}/G_u$
E_u/E_m
$G_{c,xy}$ FEM
$G_{c,xz}$ FEM
$G_{c,yz}$ FEM
$G_{c,xy}$ Analytical
$G_{c,xz}$ Analytical
$G_{c,yz}$ Analytical

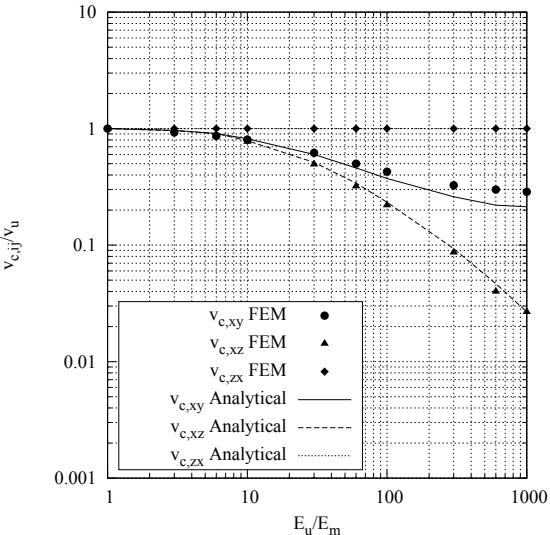
10
1
0.1
0.01
0.001
1
10
100
1000
$v_{c,ij}/v_u$
E_u/E_m
$v_{c,xy}$ FEM
$v_{c,xz}$ FEM
$v_{c,zx}$ FEM
$v_{c,xy}$ Analytical
$v_{c,xz}$ Analytical
$v_{c,zx}$ Analytical

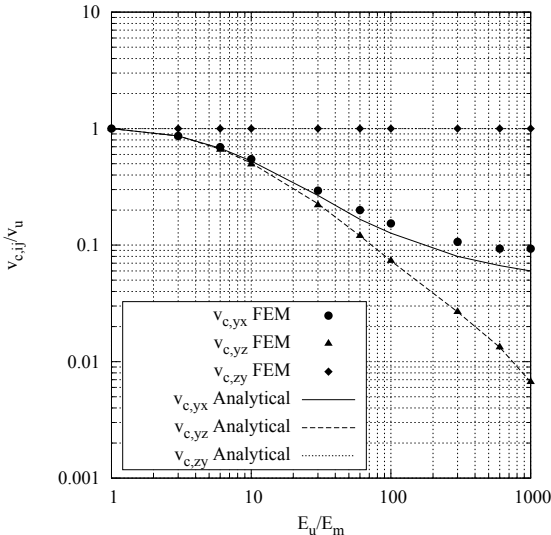
10
1
0.1
0.01
0.001
1
10
100
1000
$v_{c,ij}/v_u$
E_u/E_m
$v_{c,yx}$ FEM
$v_{c,yz}$ FEM
$v_{c,zy}$ FEM
$v_{c,yx}$ Analytical
$v_{c,yz}$ Analytical
$v_{c,zy}$ Analytical

Figure 10

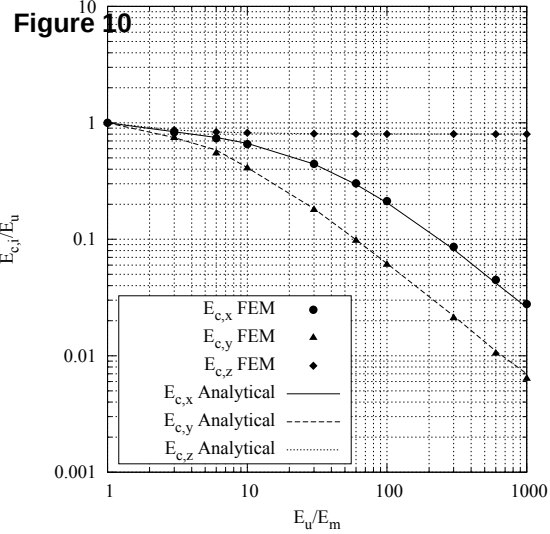
10
1
0.1
0.01
0.001
1
10
100
1000
$E_{c,i}/E_u$
E_u/E_m
$E_{c,x}$ FEM
$E_{c,y}$ FEM
$E_{c,z}$ FEM
$E_{c,x}$ Analytical
$E_{c,y}$ Analytical
$E_{c,z}$ Analytical

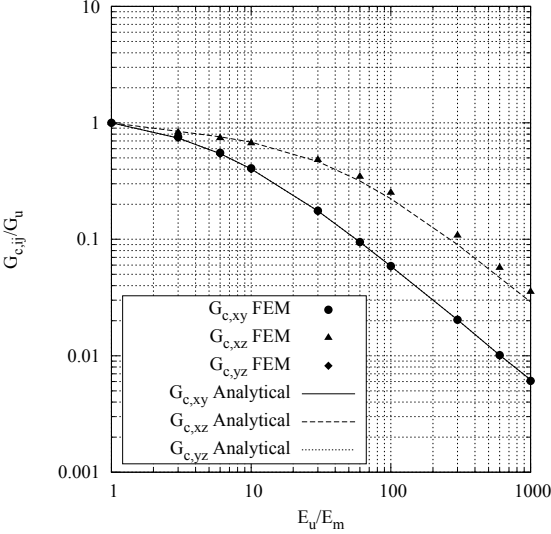
10
1
0.1
0.01
0.001
1
10
100
1000
$G_{c,ij}/G_u$
E_u/E_m
$G_{c,xy}$ FEM
$G_{c,xz}$ FEM
$G_{c,yz}$ FEM
$G_{c,xy}$ Analytical
$G_{c,xz}$ Analytical
$G_{c,yz}$ Analytical

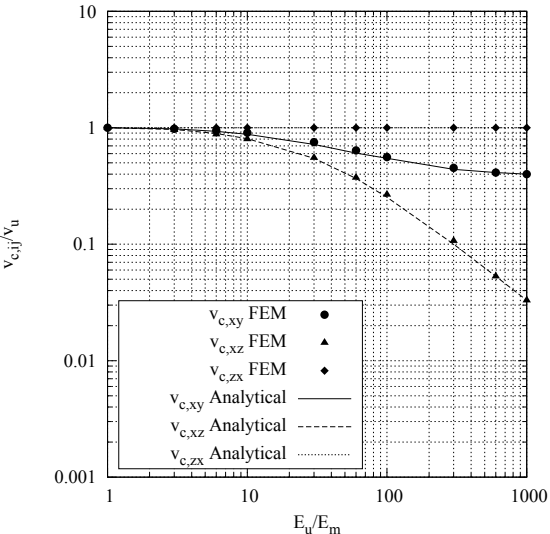
10
1
0.1
0.01
0.001
1
10
100
1000
$\nu_{c,ij}/\nu_u$
E_u/E_m
$\nu_{c,xy}$ FEM
$\nu_{c,xz}$ FEM
$\nu_{c,zx}$ FEM
$\nu_{c,xy}$ Analytical
$\nu_{c,xz}$ Analytical
$\nu_{c,zx}$ Analytical

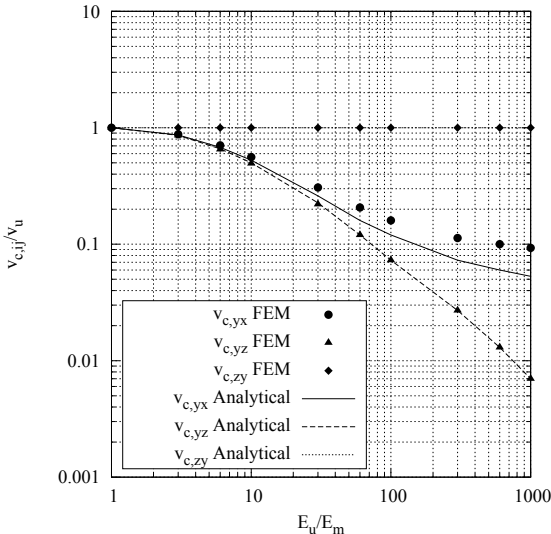
10
1
0.1
0.01
0.001
1
10
100
1000
$\nu_{c,ij}/\nu_u$
E_u/E_m
$\nu_{c,yx}$ FEM
$\nu_{c,yz}$ FEM
$\nu_{c,zy}$ FEM
$\nu_{c,yx}$ Analytical
$\nu_{c,yz}$ Analytical
$\nu_{c,zy}$ Analytical

Figure 11

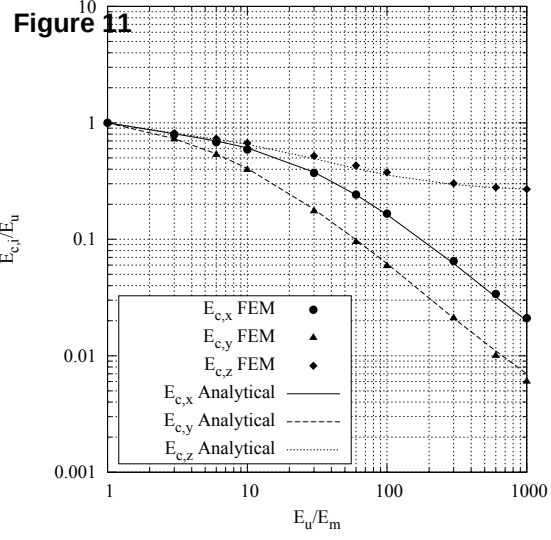
10
1
0.1
0.01
0.001
1
10
100
1000
$E_{c,i}/E_u$
E_u/E_m
$E_{c,x}$ FEM
$E_{c,y}$ FEM
$E_{c,z}$ FEM
$E_{c,x}$ Analytical
$E_{c,y}$ Analytical
$E_{c,z}$ Analytical

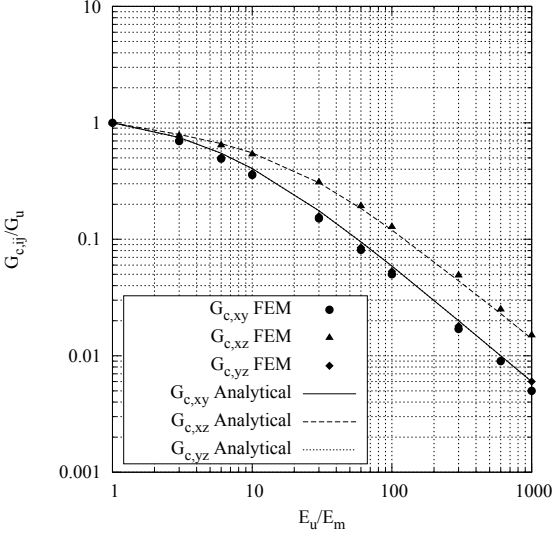
10
1
0.1
0.01
0.001
1
10
100
1000
$G_{c,ij}/G_u$
E_u/E_m
$G_{c,xy}$ FEM
$G_{c,xz}$ FEM
$G_{c,yz}$ FEM
$G_{c,xy}$ Analytical
$G_{c,xz}$ Analytical
$G_{c,yz}$ Analytical

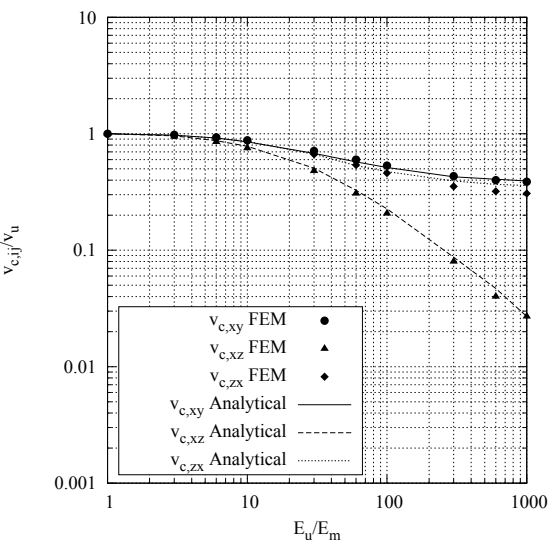
10
1
0.1
0.01
0.001
1
10
100
1000
$v_{c,ij}/v_u$
E_u/E_m
$v_{c,xy}$ FEM
$v_{c,xz}$ FEM
$v_{c,zx}$ FEM
$v_{c,xy}$ Analytical
$v_{c,xz}$ Analytical
$v_{c,zx}$ Analytical

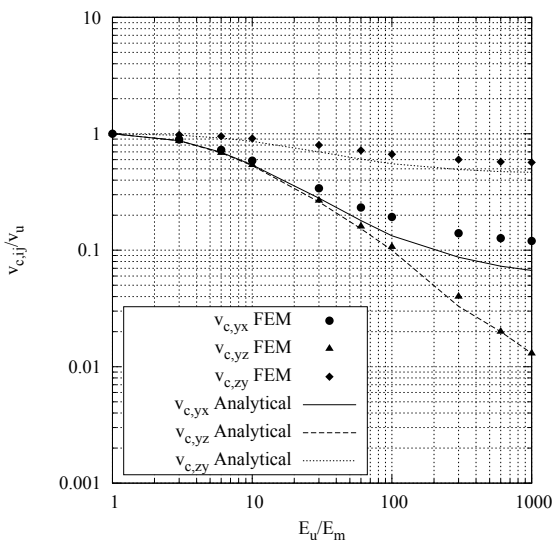
10
1
0.1
0.01
0.001
1
10
100
1000
$v_{c,ij}/v_u$
E_u/E_m
$v_{c,yx}$ FEM
$v_{c,yz}$ FEM
$v_{c,zy}$ FEM
$v_{c,yx}$ Analytical
$v_{c,yz}$ Analytical
$v_{c,zy}$ Analytical

Figure 12

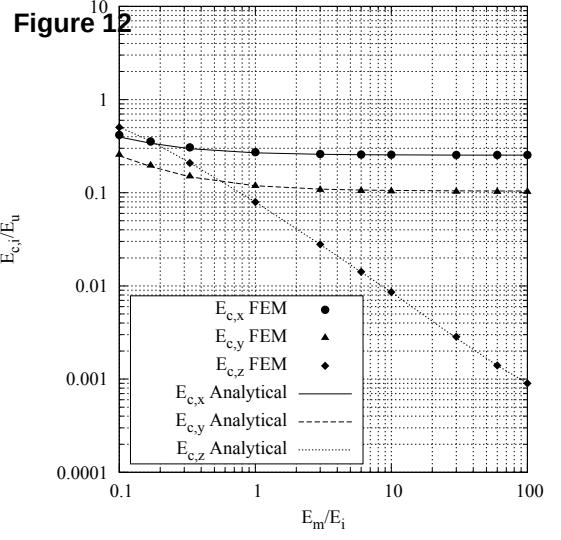
$E_{c,i}/E_u$
E_m/E_i
$E_{c,x}$ FEM
$E_{c,y}$ FEM
$E_{c,z}$ FEM
$E_{c,x}$ Analytical
$E_{c,y}$ Analytical
$E_{c,z}$ Analytical

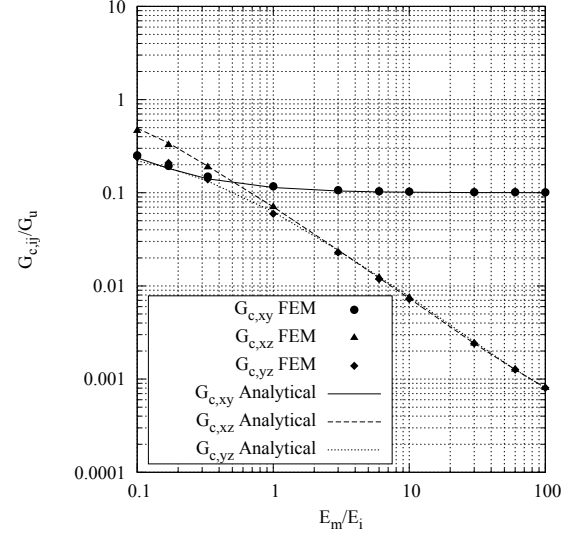
$G_{c,ij}/G_u$
E_m/E_i
$G_{c,xy}$ FEM
$G_{c,xz}$ FEM
$G_{c,yz}$ FEM
$G_{c,xy}$ Analytical
$G_{c,xz}$ Analytical
$G_{c,yz}$ Analytical

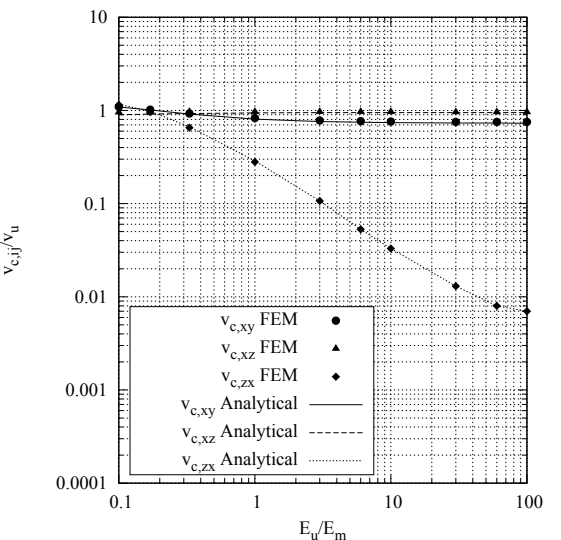
$v_{c,ij}/v_u$
E_u/E_m
$v_{c,xy}$ FEM
$v_{c,xz}$ FEM
$v_{c,zx}$ FEM
$v_{c,xy}$ Analytical
$v_{c,xz}$ Analytical
$v_{c,zx}$ Analytical

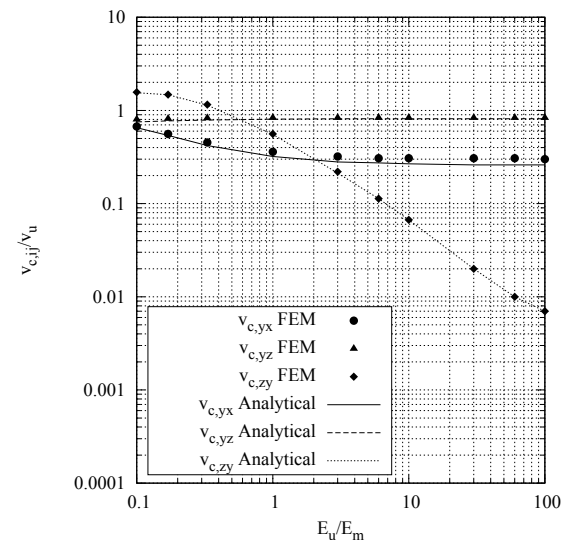
$v_{c,ij}/v_u$
E_u/E_m
$v_{c,yx}$ FEM
$v_{c,yz}$ FEM
$v_{c,zy}$ FEM
$v_{c,yx}$ Analytical
$v_{c,yz}$ Analytical
$v_{c,zy}$ Analytical

Figure 13

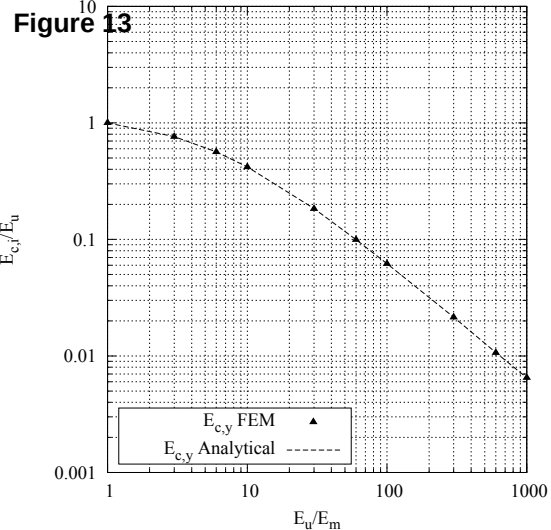
10
1
0.1
0.01
0.001
1
10
100
1000
$E_{c,i}/E_u$
E_u/E_m
$E_{c,y}$ FEM
$E_{c,y}$ Analytical

(a)

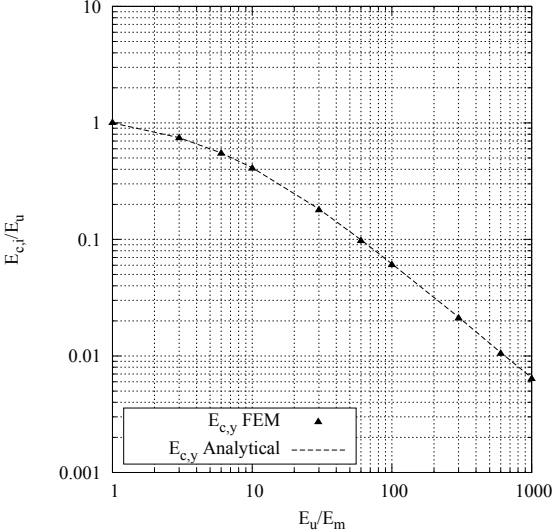
10
1
0.1
0.01
0.001
1
10
100
1000
$E_{c,i}/E_u$
E_u/E_m
$E_{c,y}$ FEM
$E_{c,y}$ Analytical

(b)

Figure 14

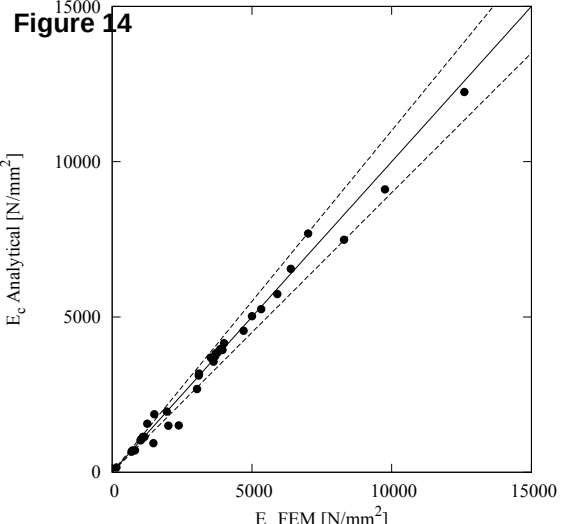
15000
10000
5000
0
0
5000
10000
15000
E_c Analytical [N/mm^2]
E_c FEM [N/mm^2]

(a)

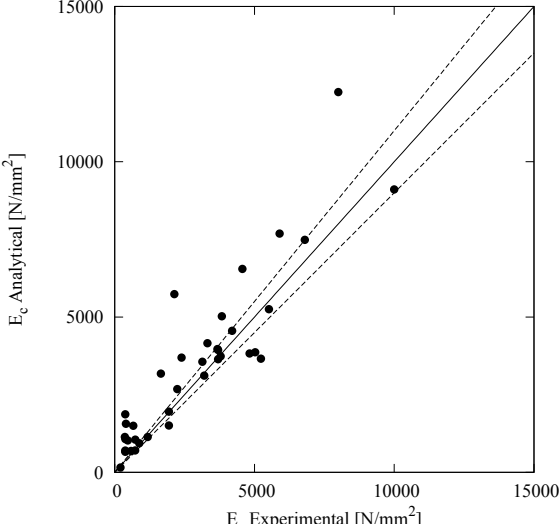
15000
10000
5000
0
0
5000
10000
15000
E_c Analytical [N/mm^2]
E_c Experimental [N/mm^2]

(b)